The Most Luminous Galaxies in the Universe

by

Ryley Hill

B.Sc., The University of British Columbia, 2015

A THESIS SUBMITTED IN PARTIAL FULFILLMENT OF
THE REQUIREMENTS FOR THE DEGREE OF

MASTER OF SCIENCE

in

The Faculty of Graduate and Postdoctoral Studies

(Astronomy)

THE UNIVERSITY OF BRITISH COLUMBIA

(Vancouver)

August 2017

Abstract

Submillimetre galaxies have become essential tools in studying the high redshift Universe. Reaching luminosities well over $10^{13}\,L_{\odot}$, they constitute the vast majority of star formation during this early epoch. Their combined infrared and submillimetre emission output is comparable in energy density to all of the optical and ultraviolet light emitted by all of the galaxies in the observable Universe.

We have used the Submillimeter Array at 860 μm to observe the brightest submillimetre sources in $4\,\mathrm{deg}^2$ of the Cosmology Legacy Survey. Previous interferometric studies have found a significant amount of multiplicity at the bright end of the single-dish number counts, suggesting a steepening in the drop-off brighter than 10 mJy, but these studies suffered from small-number statistics. We have targeted 75 of the brightest flux density-ordered single-dish SCUBA-2 sources down to approximately 10 mJy, achieving an average synthesized beam size of 2.4 arcsec and an average depth of 1.5 mJy in our primary beam-corrected maps, corresponding to 4σ detections of about 6 mJy. Our data is sufficient to distinguish between intrinsically bright galaxies and systems that break up into two $\gtrsim 6$ mJy galaxies with flux ratios less than 2 and separated by about 2 arcsec or more, corresponding to a physical distance of around 20 kpc at $z = 2$. We include in our study 28 archival observations of similar nature, bringing our sample size to 103. We statistically deboost our flux density measurements and use these to compute the cumulative and differential number counts of our sample, finding them to be consistent with previous single-dish survey number counts within the uncertainties but with a systematic offset between 2 and 20 per cent. We compute the probability that a > 10 mJy single-dish submm source resolves into two or more galaxies with a brightest to second-brightest flux density ratio less than 2 to be about 15 per cent. Assuming the remaining 85 per cent of the targets are ultra-luminous galaxies between redshifts 2 and 3, we find the surface density of $\gtrsim 500\,\mathrm{M}_{\odot}\,\mathrm{yr}^{-1}$ sources to be $8^{+2}_{-1}\,\mathrm{deg}^{-2}$ and a likely volume density of $660^{+140}_{-120}\,\mathrm{Gpc}^{-3}$.

Lay Summary

Astronomers have recently found a particularly efficient way for selecting some of the most actively star-forming galaxies in the Universe by looking for their light at special wavelengths between 0.5 and 1 mm. This new technique has led to the discovery of some of the most luminous galaxies in the known Universe. In this work I have used data from a telescope with high angular resolution to study these incredibly bright galaxies in more detail. I have shown that about 15 per cent of them are actually groups of fainter galaxies so close to one another that normal telescopes could not resolve them, while the remaining 85 per cent really are among the brightest galaxies in the Universe.

Preface

In this thesis, Chapter 2 involves work done by a collaboration of astronomers. The team members, in alphabetical order, are: Andrew W. Blain, Malcolm Bremer, Edward Chapin, Scott Chapman, Chian-Chou Chen, James S. Dunlop, Duncan Farrah, Jim Geach, Mark Gurwell, Paul Howson, Rob Ivison, Kevin Lacaille, Michal Michalowski, Ryan Perry, Glen Petitpas, Douglas Scott, Ian Smail, James Simpson, Mark Swinbank, Paul van der Werf and David J. Wilner.

Various member of this team helped write the proposal for the project (P.I. Scott Chapman), perform observations with the Submillimeter Array and reduce the data. Their work is outlined in Section 2.2. My contribution involved performing the analysis in Section 2.3 and interpreting the results given in Section 2.4, as well as coordinating the team's work and writing the full document. A version of this chapter is being prepared for submission to Monthly Notices of the Royal Astronomical Society.

Table of Contents

List of Tables

List of Figures

List of Abbreviations

Telescopes/Instruments/Satellites	
Atacama Large Millimeter/submillimeter Array	ALMA
Astronomical Thermal Emission Camera	AzTEC
Balloon-borne Large Aperture Submillimeter Telescope	BLAST
Cosmic Background Explorer	COBE
Diffuse Infrared Background Experiment	DIRBE
Far-Infrared Absolute Spectrophotometer	FIRAS
Infrared Array Camera	IRAC
Infrared Astronomy Satellite	IRAS
Large Apex Bolometer Camera	LABOCA
Multiband Imaging Photometer for *Spitzer*	MIPS
Plateau de Bure Interferometer	PdBI
Submillimeter Common User Bolometer Array/-2	SCUBA/-2
Submillimeter Array	SMA
Spectral and Photometric Imaging Receiver	SPIRE
United Kingdom Infrared Telescope	UKIRT
Very Large Array	VLA

Surveys/Fields	
Akari-North Ecliptic Pole	*Akari*-NEP
ALMA survey of LESS	ALESS
Cosmology Legacy Survey	CLS
Cosmic Evolution Survey	COSMOS
Extended *Chandra* Deep Field-South	E-CDF-S
Extended Groth Strip	EGS
Great Observatories Origins Deep Survey-North	GOODS-N
LABOCA E-CDF-S Submillimeter Survey	LESS
Lockman Hole North	LHN
Small Selected Area 22	SSA22
UKIRT Infrared Deep Sky Survey Ultra-Deep Survey	UDS

Astronomical terms	
cosmic infrared background	CIB
cosmic optical background	COB
declination	Dec
full-width half-maximum	FWHM
infrared	IR
right ascension	RA
spectral energy distribution	SED
star-formation rate	SFR
submillimetre galaxy	SMG
signal-to-noise ratio	S/N
submillimetre	submm

Acknowledgements

Several telescope facilities were used to gather data for this thesis. The James Clerk Maxwell Telescope is now operated by the East Asian Observatory on behalf of The National Astronomical Observatory of Japan, Academia Sinica Institute of Astronomy and Astrophysics, the Korea Astronomy and Space Science Institute, the National Astronomical Observatories of China and the Chinese Academy of Sciences (Grant No. XDB09000000), with additional funding support from the Science and Technology Facilities Council of the Kingdom and participating universities in the United Kingdom and Canada. The Submillimeter Array is a joint project between the Smithsonian Astrophysical Observatory and the Academia Sinica Institute of Astronomy and Astrophysics and is funded by the Smithsonian Institution and the Academia Sinica. The author wishes to recognize and acknowledge the very significant cultural role and reverence that the summit of Maunakea has always had within the indigenous Hawaiian community. We are most fortunate to have the opportunity to conduct observations from this mountain. This work was supported by the Natural Sciences and Research Council of Canada.

Chapter 1

Introduction

Submillimetre galaxies (SMGs) are the most luminous and productive galaxies in the Universe. Understanding their nature and place in the sequence of galactic evolution has been at the forefront of astronomical research since their discovery, resulting in many key insights on the cosmic history of star formation, galaxy formation and galaxy clustering – covering nearly all scales of structure formation.

During the 1980s, the Infrared Astronomy Satellite (IRAS; Neugebauer et al. 1984) opened a new window for studying galaxies at mid- to far-infrared wavelengths. IRAS was the first instrument to catalogue a statistically significant population of extremely bright extragalactic infrared sources, defined as galaxies with luminosities greater than $10^{11}\,L_{\odot}$ (Sanders et al. 2003). Equipped with samples of highly luminous, vigorously star-forming local galaxies, researchers were naturally led to predict the existence of a population of highly luminous, vigorously star-forming distant and abundant galaxies, theorizing that the known luminous galaxies were in fact left over from a much vaster population responsible for the majority of star formation in the Universe.

The first hint that such a population existed came from measurements of the cosmic infrared background (CIB) – the sum of all infrared (IR, $1\,\mu$m – $200\,\mu$m) and submillimetre (submm, $200\,\mu$m – 1 mm) radiation emitted from extragalactic sources averaged over the entire sky – with the Far-Infrared Absolute Spectrophotometer (FIRAS; Mather et al. 1993) and the Diffuse Infrared Background Experiment (DIRBE; Silverberg et al. 1993) aboard the Cosmic Background Explorer (COBE). What FIRAS and DIRBE were able to show was that not only was the CIB comparable in energy density to its optical counterpart (the cosmic optical background, or COB), but that much less than 10 per cent of it had actually been resolved into galaxies with IRAS (Hauser et al. 1998).

The implications of this observation were tremendous; a significant amount of the star-formation activity of the Universe must have taken place in very distant, very dusty galaxies, where optical and ultraviolet light had been absorbed and re-emitted in the IR and submm. Detecting and character-

izing the population responsible for this radiation became a compliment to studying the origins of the stars and galaxies that populate the night sky today. This inevitably led to the development of submm astronomy, and the detailed study of SMGs.

1.1 Observing in the submm waveband

The history of extragalactic submm astronomy is a short one, dating only as far back as the mid-1990s. The reason for such a late blooming of an otherwise fruitful subject can be attributed to technology. At the time it was widely speculated that an enormous number of distant, dust enshrouded galaxies existed in the far IR and submm. Individual high redshift objects were already known from IRAS follow-up work, but were rare, and there was no way to study large samples of such galaxies due to the sensitivity required to actually detect them.

First, there is the question of resolution. The basic resolving power of a dish goes as $1.22\,\lambda/D$, where λ is the wavelength of light being observed and D is the diametre of the dish. To obtain something like half an arcminute of resolution at 850 μm, one must have a dish about 10 m across. This would be useful for answering many scientific questions, but obtaining arcsecond and sub-arcsecond resolution, necessary for resolving individual SMGs, would require a dish over 30 times larger! As we shall see in the proceeding section, this problem can be addressed with a technique known as interferometry, which takes advantage of the interference patterns created by coherently using an array of individual dishes.

Second, one must deal with the Earth's atmosphere, which is nearly opaque at submm wavelengths. This is due to the abundance of water vapour, which has particularly strong absorption at these wavelengths. This means either finding a consistently dry location, or performing observations from space. The latter solution is the more difficultand expensive approach – imagine what would be required to place a perfectly curved, 15-m dish into orbit, or to set up a sophisticated interferometric system in space. It is for this reason that submm observatories are usually built high atop mountains, where the atmosphere is thin enough to permit observations through various 'windows'. These windows are bands located between the water vapour absorption lines, and are centred around 350 μm, 450 μm, 750 μm, 850 μm and 1.1 mm, as shown in Figure 1.1.

Fortunately, there is a phenomenon present that helps in the detection of high redshift SMGs, known as the negative K-correction. A K-correction

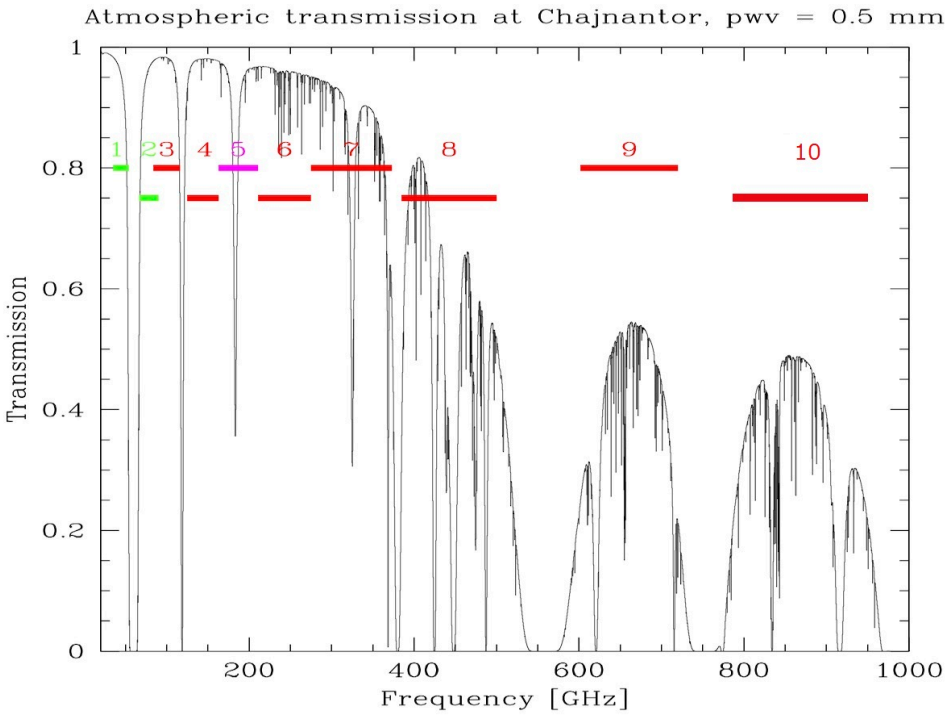

Figure 1.1: Transmission function of Earth's atmosphere at the Llano de Chajnantor Observatory on the Atacama Plateau in northern Chile. The elevation of the observatory is 5000 m above sea level, crucial for minimizing the amount of water vapour above the telescope. Strong absorption lines can be seen at 600 GHz (500 μm) and 800 GHz (375 μm), while observational 'windows' are present at 850 GHz (350 μm), 650 GHz (450 μm), 400 GHz (750 μm), 350 GHz (850 μm), and 270 GHz (1.1 mm). The red, purple and green segments represent a submm telescope's observational bands, which roughly correspond to these windows. Figure taken from the ALMA Cycle 5 Technical Handbook (2017).

is added to an object's absolute magnitude to convert its flux density from the observed frame to the rest frame; it is thus useful for extragalactic objects with significant redshifts. One generally expects the K-correction to be positive for a given object, because it should become fainter the more it gets redshifted. But the opposite happens in the submm. This can be seen by considering thermal radiation from a cool ($\simeq 30\,\mathrm{K}$) blackbody. IR and optical emission lies on the Wien portion of the spectral energy distribution (SED), where the intensity decreases steeply with decreasing wavelength. When an object becomes redshifted, its SED is sent to larger wavelengths in the observing frame, and so a given wavelength in the observing frame now corresponds to a much shorter wavelength in the rest frame, which has a significantly lower intensity. K-corrections are said to be 'positive' if the intensity decreases with increasing redshift, hence a positive K-correction in this case. For submm observers, these wavelengths lie on the Rayleigh-Jeans side of the SED, where instead intensity increases with decreasing wavelength. This means that in redshifting an object, it becomes brighter, and hence it has a negative K-correction. This is very beneficial for observing SMGs, which exist at high redshifts and turn out to have almost the same apparent brightness over a wide range of redshifts.

1.2 The spectral energy distribution

We learn a lot about the physical conditions in SMGs from modelling their SEDs. From the SED of an SMG one can estimate quantities such as the star-formation rate (SFR), the mean dust temperature and the dust mass. Here we will describe some of the more widely used models, and the physical motivation behind them.

The modified blackbody equation is by far the most widely used model for the SED of an SMG (Figure 1.2). To start, this model is motivated by the observation that the majority of radiation emitted from these galaxies is due to dust grains. These dust grains have absorbed the majority of the optical and ultraviolet light of the surrounding stars, and are approximately re-emitting this starlight as described by the Planck function $B_\nu(T)$. The temperature parameter T used here in the Planck function is a collective average of the temperatures of the dust grains making up the SMG (and should not be interpreted as the true temperature of the dust).

Next, to 'modify' the blackbody, we note that the emitted radiation must pass through a medium with a finite optical depth $\tau(\nu)$, which leads to some extinction by a factor $1 - e^{-\tau(\nu)}$. Therefore, the expression for the intensity

of an SMG takes on the form

$$S_\nu \propto (1 - e^{-\tau(\nu)}) \frac{\nu^3}{e^{h\nu/kT} - 1}. \tag{1.1}$$

Lastly, the optical depth is modelled as power law,

$$\tau(\nu) = \left(\frac{\nu}{\nu_0}\right)^\beta, \tag{1.2}$$

where ν_0 is a characteristic frequency at which the optical depth is 1 (causing the emitted intensity to fall by a factor of $1 - e^{-1} \simeq 0.63$) and β is known as the spectral emissivity index. When the optical depth is small (typically the case in dusty galaxies) we can write $1 - e^{-\tau(\nu)} \simeq \tau(\nu)$ to obtain the commonly encountered power-law modification to $B_\nu(T)$. Of course this has the downside of introducing two additional free parameters, but the characteristic frequency and spectral index are usually set to values around 3 THz and 1.5, respectively. These values are somewhat based on ideal theoretical considerations but may vary among galaxy types; values of ν_0 have been measured at the 1.5 THz level (Rangwala et al. 2011), while β can range from 1 to 2 if one allows it to be a free parameter (Chapin et al. 2011). Best-fit temperature values obtained from this model generally range from 30 – 40 K (e.g. Chapman et al. 2005).

Albeit the most common model, due to its simplicity and parameterization, other more complicated models are sometimes necessary. For example, it is known that most SMGs exhibit a mid-IR excess due to a component of clumpy, hotter than average dust. This can be taken into account by introducing two modified blackbodies with variable temperatures (as considered, for instance, in Kirkpatrick et al. 2012), or by introducing a cutoff frequency where the modified blackbody becomes a strict power law (see Roseboom et al. 2013, for example). Of course there are also many more numerical fitting algorithms, which can contain all sorts of astrophysical phenomena such as radiative transfer, chemical evolution and energy balance (e.g., Siebenmorgen and Krügel 2007; Rieke et al. 2009; Noll et al. 2009). In detail an SED will have emission lines and various other features; however, this level of complexity is unnecessary when we are only dealing with broad-band photometry measurements.

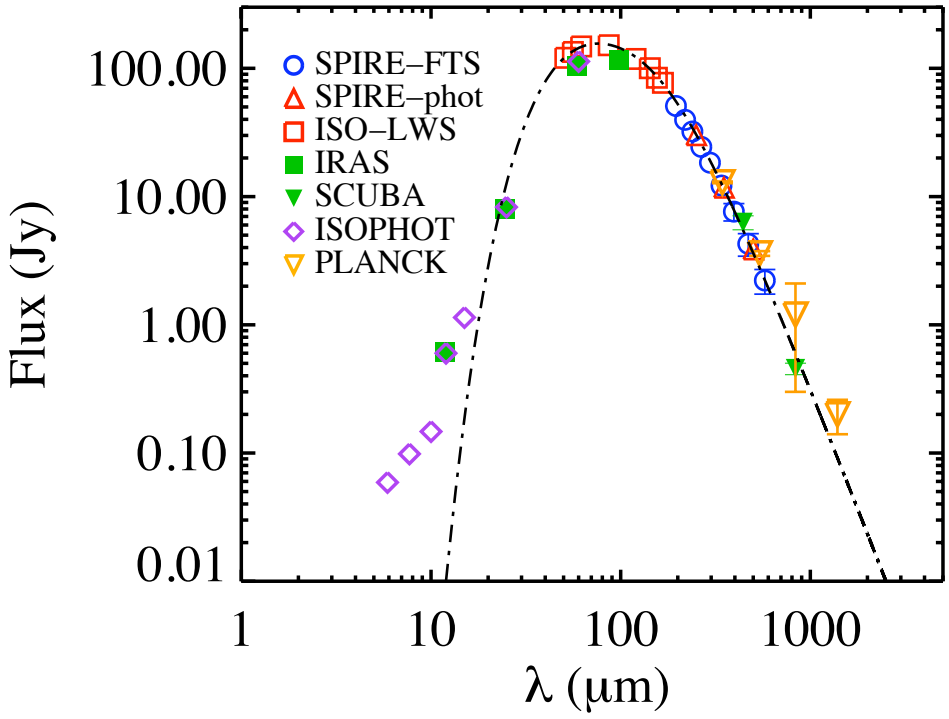

Figure 1.2: Modified blackbody SED. The example shown here is for ARP 220, the nearest ultra-luminous infrared galaxy to the Milky Way. The best-fit parameters in this case are $T = 66.7\,\mathrm{K}$, $\nu_0 = 1.277\,\mathrm{THz}$ and $\beta = 1.83$. ARP 220 is thought to contain a burried active galactic nuclei, hence it has a value of T larger than the mean of 40 K. Figure taken from Rangwala et al. (2011).

1.3 Redshift distribution

Redshifts are of utmost importance for studying galaxies, since we need this information to convert observed quantities to intrinsic properties. As we know, SMGs are typically very distant and hence seen as they were billions of years ago. But just how young, and how distant? Did they all form around the same time? When were the first SMGs? And were they different than the galaxies that formed later? These are questions which can be answered by studying their redshift distribution.

Redshifts come in two flavours: spectroscopic and photometric. The former technique relies on the detection of known emission lines, and the shift in wavelength can be used to calculate the recessional speed (i.e. redshift). This method is always extremely precise, but expensive in telescope time. The latter technique involves assuming a rest frame SED, and calculating the shift from the measured SED. This method is much easier because it only requires a few flux density measurements, but uncertainties in the SED model mean that it is much less precise.

On top of the lack of *a priori* redshift knowledge, measuring photometric redshifts of SMGs turns out to be quite difficult for two additional reasons: (1) being quite dusty by nature, SMGs obscure much of the classically bright optical and ultraviolet emission lines; and (2) the inability of single dish instruments to pinpoint SMGs accurately enough to locate their counterparts at other wavelengths. Yet measuring photometric redshifts is also difficult. Since the standard approach to modelling SMG SEDs is the modified blackbody, there is an inherent degeneracy between the temperature and the redshift (increasing the temperature has the same effect as decreasing the redshift, the SED moves to shorter wavelengths). But using additional knowledge, researchers have come up with some clever ways around these issues (e.g., Barger et al. 2012; Chen et al. 2016).

Many studies have looked at the redshift distribution of SMGs (e.g., Chapman et al. 2005; Wardlow et al. 2011; Chen et al. 2016). An example is shown in Figure 1.3. Results generally show a peak between $z = 2$ and $z = 2.5$, no more than 10% at $z < 1$, and a small tail out to $z \approx 5$. It is evident that there is a special peak epoch for SMGs, implying that the Universe underwent a massive star-forming period between redshift 2 and 3. This is an important clue to understanding the cosmic history of star formation.

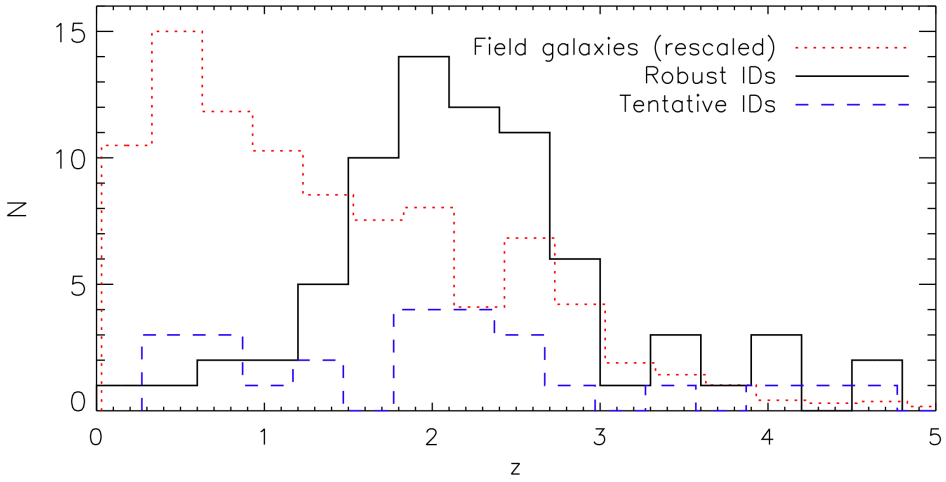

Figure 1.3: Example SMG redshift distributions, taken from Wardlow et al. (2011). The 'robust IDs' are SMGs with radio detected counterparts, which the 'tentative IDs' lack. This plot clearly demonstrates that the distribution of SMGs is highly concentrated about redshift 2.5 and is significantly different from randomly selected field galaxies, which peak around redshift 0.5.

1.4 Driving mechanisms

With some information about their physical properties, we can then ask what mechanism is fuelling the intense luminosities and SFRs seen in SMGs. Two scenarios dominate the discussion in the literature: (1) major mergers cause significant perturbations in the interstellar gas, which lead to exceptional increases in SFRs; and (2) the intense luminosities observed are in fact a normal part of galaxy evolution and are caused by standard accretion of intergalactic gas in the dense, early Universe.

The former, major merger framework does well in that simulations of these events are capable of reproducing the correct IR luminosities (and, by extension, SFRs). On the downside, theoretical calculations do not predict enough major mergers to occur around redshifts 2–3 to account for the number density of SMGs observed on the sky (e.g. Narayanan et al. 2010). On the other hand, the quiescent accretion framework does a poor job at obtaining high enough SFRs. But, if certain unconventional assumptions about the initial conditions are made, then correct SFRs and number densities can be obtained (e.g. Baugh et al. 2005).

More recent simulations are beginning to suggest that the answer involves a combination of these two scenarios. It is suggested that many SMGs are made up of a few to many smaller galaxies, which, when seen through a single dish telescope, are merged into a single massive and highly luminous galaxy. The smaller galaxies still have high SFRs, but these can be duplicated through a combination of accretion of extragalactic gas and perturbations from interactions (Davé et al. 2010; Narayanan et al. 2015). Despite the attractiveness of this idea, there still lacks observational evidence to back up various details.

One basic question remains: how luminous can individual SMGs get? Once we have answered this we can determine wheather current theoretical models are able to predict them.

Chapter 2

High-resolution imaging of bright submillimetre sources from the SCUBA-2 Cosmology Legacy Survey with the SMA

2.1 Introduction to multiplicity in SMGs

The emergence of submm astronomy has led to the discovery of a cosmologically important population of SMGs, which appear to be among the earliest and most actively star-forming galaxies in the Universe (e.g., Blain et al. 2002; Chapman et al. 2005; Magnelli et al. 2012; Swinbank et al. 2014; MacKenzie et al. 2017; Michałowski et al. 2017; Simpson et al. 2017). While single dish observations of SMGs using facilities like the Submillimeter Common User Bolometer Array (SCUBA; Holland et al. 1999), SCUBA-2 (Holland et al. 2013), the Balloon-borne Large Aperture Submillimeter Telescope (BLAST; Pascale et al. 2008), the Astronomical Thermal Emission Camera (AzTEC; Wilson et al. 2008), the Large Apex Bolometer Camera (LABOCA; Siringo et al. 2009), and the space-based Spectral and Photometric Imaging Receiver (SPIRE; Griffin et al. 2010) on board the *Herschel* satellite were able to greatly increase our knowledge about the evolution of star formation in the Universe (e.g., Blain et al. 1999; Magnelli et al. 2013; Gruppioni et al. 2013; Swinbank et al. 2014; Koprowski et al. 2017), their connection with today's galaxies remains unclear, although evidence is mounting that they are progenitors of massive elliptical galaxies (e.g., Lilly et al. 1999; Scott et al. 2002; Genzel et al. 2003; Swinbank et al. 2006; Toft et al. 2014; Simpson et al. 2014; Koprowski et al. 2014; van Dokkum et al. 2015; Koprowski et al. 2016; Michałowski et al. 2017; Simpson et al. 2017).

There is also debate about whether or not mergers are important for

SMGs. Many simulations require mergers to achieve the observed massive SFRs (e.g., Narayanan et al. 2015) while others do not (e.g., Davé et al. 2010), and on the other hand, observations of physically associated pairs of SMGs with disturbed gas motions indicate that mergers are present (e.g., Tacconi et al. 2008; Engel et al. 2010; Chen et al. 2015), while ultraluminous SMGs have been seen that lack such evidence (e.g., Targett et al. 2013; Michałowski et al. 2017). Progress is impeded by the sub-optimal angular resolution offered by single dish telescopes at submm wavelengths, which typically ranges between 10 arcseconds and half an arcminute. At these scales, source blending becomes a significant problem, and optical/IR counterparts cannot be easily identified (with the notable exception of radio-bright SMGs; see e.g., Ivison et al. 2002, 2007; Biggs et al. 2011).

Submm interferometry offers the arcsecond resolution necessary to accurately identify and pin-point individual submm galaxies. The Plateau de Bure Interferometer (PdBI; Guilloteau et al. 1992), the Submillimeter Array (SMA; Ho et al. 2004) and the Atacama Large Millimeter/submillimeter Array (ALMA; Wootten and Thompson 2009) have greatly aided in the localisation of counterparts and further characterization of SMGs. These were the first facilities to conclusively show that many SMGs exhibit multiplicity (e.g., Iono et al. 2006; Younger et al. 2007, 2009; Wang et al. 2011; Smolčić et al. 2012; Hodge et al. 2013; Simpson et al. 2015; Miettinen et al. 2015), where one bright submm source resolves into two or three individual SMGs. However, it was difficult to demonstrate this multiplicity for the most extreme SMGs due to their sparsity in the sky and an interferometre's limited field of view.

Large single-dish submm surveys (e.g., Scott et al. 2002; Greve et al. 2004; Wang et al. 2004; Coppin et al. 2006; Bertoldi et al. 2007; Weiß et al. 2009; Oliver et al. 2010; Valiante et al. 2016; Geach et al. 2017), followed up by interferometers, have been important for addressing the issue of multiplicity as they provide substantial catalogues of bright SMGs across continuous patches of sky that interferometres can follow-up. These types of studies are primarily driven by their sensitivity (being unable to detect, for example, very faint dwarf galaxies), but they are able to distinguish between intrinsically bright galaxies and systems comprising of two or more galaxies with similar flux densities that would lead to a significant overestimation from single-dish measurements. For example, Barger et al. (2012) used the SMA to observe $16 > 3$ mJy sources detected with SCUBA-2 in the Great Observatories Origins Deep Survey-North field (GOODS-N; Wang et al. 2004), finding that three resolved into multiple SMGs. Similarly, Smolčić et al. (2012) used the PdBI at 1.3 mm to target $28 > 5$ mJy sources detected by

LABOCA at 870 μm in the Cosmic Origins Survey field (COSMOS; Scoville et al. 2007), and found that six of them resolved into more than one SMG. A larger survey of the Extended *Chandra* Deep Field-South (E-CDF-S; Lehmer et al. 2005) using LABOCA (the LESS survey; Weiß et al. 2009) was followed up with ALMA (the ALESS survey; Hodge et al. 2013), who observed 126 sources > 3.5 mJy and found that 24 out of the 69 most robust observations showed multiple SMGs. Similar to the previous multiplicity studies, Simpson et al. (2015) used ALMA to follow-up 30 of the brightest (> 5 mJy) sources detected in the United Kingdom Infrared Telescope (UKIRT; Casali et al. 2007) Infrared Deep Sky Survey-Ultra-Deep Survey field (UKIDSS-UDS; Lawrence et al. 2007), mapped by SCUBA-2 as part of the Cosmology Legacy Survey (CLS; Geach et al. 2017), and found that 18 sources break up into more than two SMGs. While these types of surveys have begun to reach statistically significant numbers of samples, they nonetheless lack large numbers of the brightest (> 10 mJy) single dish detected sources; for example, the LESS survey contained six sources brighter than 10 mJy, and the catalogue from Simpson et al. (2015) contained five sources brighter than 10 mJy.

To date, the largest submm survey of the extragalactic sky is the complete CLS, encompassing 5 deg^2 of the sky over seven cosmological fields, namely the UKIDSS-UDS, COSMOS, the *Akari*-North Ecliptic Pole (*Akari*-NEP; Lee et al. 2009), the Extended Groth Strip (Groth et al. 1994), the Lockman Hole North (Dickey and Lockman 1990), the Small Selected Area 22 (SSA22; Lilly et al. 1991) and the GOODS-N. The CLS detected over 2800 submm sources above 3.5σ, about 50 of which are brighter than 10 mJy. This survey is therefore well-suited to study the properties of multiplicity in the brightest SMGs known to exist.

Here we present results from the largest yet interferometric follow-up programme of the brightest submm galaxies, selected from 80 per cent of the available area in the CLS survey. We have imaged 75 SCUBA-2 sources whose flux densities are $\gtrsim 8$ mJy with 2.4 arcsec resolution using the SMA in order to measure the importance of multiplicity in this bright population of SMGs. In Section 2.2 we describe our target selection, data reduction and source extraction procedure, in Section 2.3 we correct our flux density measurements for flux boosting and compare our data to the CLS catalogue to asses the reliability of our sample, and in Section 2.4 we examine the completeness of our sample, present number counts, and discuss the effects of multiplicity on the population of bright SMGs seen in our data. The results are summarized in Section 2.5.

2.2 Observations

2.2.1 Target selection and observations

In our observing programme we used the SMA in the compact configuration at 860 μm to investigate bright sources in five out of the seven CLS fields, namely UKIDSS-UDS, COSMOS, the Extended Groth Strip, the Lockman Hole North, and SSA22 (hereafter the UDS, COSMOS, EGS, LHN and SSA22 fields, respectively). Combined, these fields make up about 4 deg^2 and contain roughly 2500 SCUBA-2 sources, 40 being brighter than 10 mJy. Our initial aim was to target and resolve all sources down to 10 mJy to determine the effects of multiplicity on the bright end of the submm number count with good statistical significance. At the time these observations were first proposed, the CLS had not yet been completed, being at that point shallower than the final maps published in Geach et al. (2017). This led to several cases where either a proposed SCUBA-2 target ended up fainter than expected, or an originally faint SCUBA-2 source ended up being brighter than 10 mJy. When selecting targets we only considered the measured (uncorrected) SCUBA-2 flux densities, which are believed to be boosted by positive noise and faint background galaxies that on average add a positive bias to the flux densities and are statistically corrected for in the final CLS catalogue in Geach et al. (2017). This effect resulted in more examples of apparently bright SCUBA-2 sources ending up being fainter in the final list.

There are several submm interferometric data sets from the SMA and ALMA in the literature that we did not re-observe in our programme. In particular, Simpson et al. (2015) carried out a follow-up campaign of 30 high signal-to-noise ratio (S/N) CLS sources in the UDS field with ALMA at 870 μm, and Younger et al. (2007, 2009) selected the highest significance sources in an AzTEC survey of the COSMOS field (Scott et al. 2008) for follow-up with the SMA at 890 μm. Additionally, there is a single strong gravitational lense in the UDS field, dubbed 'Orochi', reaching an 850-μm flux density of 52.7 mJy in the SCUBA-2 map; this source was followed up by Ikarashi et al. (2011) with the SMA at 860 μm in part of a detiled multiwavelength study. We have included 28 observations from these works into our analysis, which is detailed in Section 2.3.4.

Our final SMA follow-up campaign sample consisted of 75 total targets; 23 in the UDS field, nine in the SSA22 field, 16 in the COSMOS field, 18 in the LHN field and nine in the EGS field. These sources were the brightest sources down to approximately 10 mJy, except in the UDS field where we probed sources with flux densities down to about 8 mJy. In Fig. 2.1 we

show the SCUBA-2 deboosted flux density distribution from our parent CLS sample, with the distribution of our targets and the distribution of our full catalogue (including archival sources) overlaid. This shows the completeness of our selection, which we quantify later in Section 2.3.4.

We note that we followed up two sources in the EGS field and two sources in the COSMOS field that ended up excluded from the final CLS catalogue. These four sources lie near the edge of the EGS and COSMOS maps, where the rms is higher, and were thus excluded from the area used to define the final CLS regions. While these four sources do not appear in our study, we nonetheless report them here for completeness.

The observations were carried out over a period of two years between November 2014 and November 2016. We set up the SMA in the compact configuration tuned to 345 GHz and nominally used all eight available 6-m dishes. The synthesized beam achieved in this set up is about 2.4 arcsec. Flux densities were calibrated using Uranus, Neptune, Callisto or Titan, depending on availability and proximity to the given target. Our aim was to detect 100 per cent of a target's SCUBA-2 flux density at 4σ, requiring depths varying from about 0.7 mJy to 2 mJy.

2.2.2 Source detections

The data were reduced using standard `CASA` calibration and `CLEAN`ing routines, with Briggs weighting and a robustness parameter of 0, and primary beam corrected. The mean depth achieved in our data was 1.5 mJy (calculated within 25 arcsec of the centre of the primary beam-corrected maps), varying between 0.7 mJy and 2.4 mJy, with one map at the 2.8 mJy level and one map at the 3.2 mJy level. We set a detection threshold of $> 4\sigma$ peaks in our maps. In the UDS field we detected 21 out of the 23 SCUBA-2 sources we followed-up; none of these 21 sources were seen to break up into two components, and two sources remained undetected. Within the COSMOS field, our SMA observations detected a total of 13 galaxies from the 16 SCUBA-2 sources: one source broke up into two galaxies; and in four sources we found no peaks greater than 4σ. Of the nine SCUBA-2 sources targeted in the SSA22 field, four were not detected above the 4σ level in the SMA maps, and in the remaining five we found single galaxies. In the LHN field we found 18 galaxies from our targeted sample of 18 SCUBA-2 sources. Of these 18 detections two are SCUBA-2 sources that break up into two galaxies, and in two cases we did not find any galaxies. In the EGS field we have detected single galaxies for all nine SCUBA-2 sources. We also report galaxy detections of all four of the SCUBA-2 sources we followed up

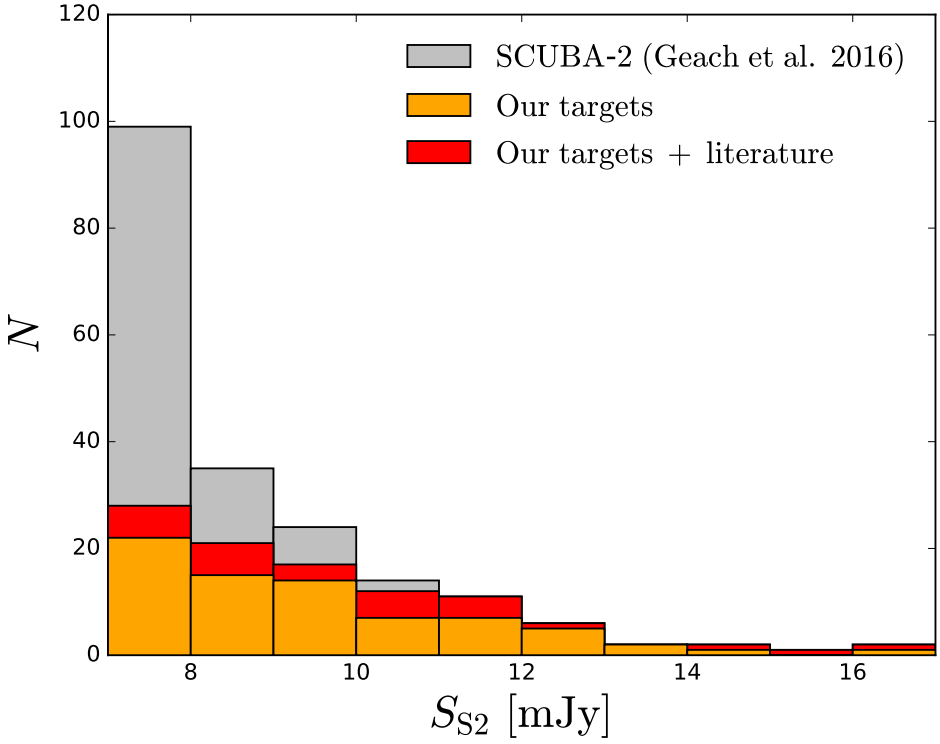

Figure 2.1: Histogram showing the deboosted flux density distribution of the parent SCUBA-2 CLS survey from Geach et al. (2017), our 75 targets, and our full catalogue including these 75 targets and 28 archival sources from Simpson et al. (2015), Younger et al. (2007), Younger et al. (2009) and Ikarashi et al. (2011), which are included in our counts analysis. Our sample is a nearly complete selection of single-dish SCUBA-2 sources with flux densities brighter than 10 mJy.

outside of the boundary of the CLS regions, and note that none resolved into multiples.

Overall we detected 66 submm galaxies in 75 SMA pointings above a 4σ depth of about 6 mJy. These detections are summarized in Tables A.1–A.5, where we provide the positions of both the SCUBA-2 sources and our SMA detections, the measured and deboosted SCUBA-2 flux densities of each target as $S_{\rm S2}^{\rm obs}$ and $S_{\rm S2}$, respectively, and our measured flux densities as $S_{\rm SMA}^{\rm obs}$. For undetected sources, we report the 4σ flux density limit achieved by our observations instead. In each field, we sort sources in descending order of their deboosted SCUBA-2 flux density.

2.2.3 Source IDs

Spitzer-Infrared Array Camera (IRAC) 3.6μm, Multiband Imaging Photometer for *Spitzer* (MIPS) 24μm and Very Large Array (VLA) 1.4 GHz imaging exists for 38 of our targets. In Fig. B.1 we show SMA contours overlaid over these multiwavelength data along with SMA contours. We can see that there are IR/radio sources coincidental with nearly all of our SMA positions to within 1 arcsec, showing the generally high quality of our SMA detections, complete with robustly identified conterpart galaxies. The multiwavelength properties of these galaxies will be investigated in future work.

There are several cases where we have detected an SMA peak between 3 and 4σ that matches both an IR and a radio counterpart. Specifically, we see this with LHN11 and LHN12, where SMA flux densities were measured to be 7.0 ± 1.8 mJy and 6.0 ± 2.0 mJy, respectively. In addition, we have found two SMA peaks with flux densities of 5.1 ± 1.5 mJy and 4.5 ± 1.5 mJy within 3 arcsec of LHN09, each directly overlapping with an IR counterpart and a radio counterpart. In contrast, our remaining SMA data lacking 4σ peaks do not show any peaks $> 3\sigma$ overlapping with IR or radio sources. We have therefore included LHN11 and LHN12 in our analysis, and we report the detection of a triple system in LHN09. These sources are included in Table A.4, with an indication that the detections are less than our 4σ flux density threshold.

It is worth noting that in the COSMOS field, out of the 18 SCUBA-2 sources found by Michałowski et al. (2017) to have multiwavelength counterparts and included in our sample, all were confirmed by our SMA imaging. In the UDS field, out of 35 SCUBA-2 sources overlapping between our two studies, 31 were confirmed (89 per cent), consistent with the reliability of $\simeq 92$ per cent measured by Michałowski et al. (2017) based on the ALMA

data of Simpson et al. (2015). Similarly, Chen et al. (2015) was able to identify multiwavelength counterparts for $\simeq 79$ per cent of the SCUBA-2 sources detected in the Extended *Chandra* Deep Field South, consistent with our observations.

2.3 Analysis

2.3.1 Flux boosting

The effects of selection biases, particularly 'flux boosting', on our results are complicated. This is because we picked bright outliers in large SCUBA-2 maps, followed them up with the SMA, and then observed them at higher resolution. Because of this complexity, we put considerable effort into simulating our observing and analysis procedure. The effect of flux boosting results from the statistical nature of measuring flux densities in a noisy map where there are many more faint sources than bright ones. This effect will tend to scatter sources to higher flux densities rather than lower ones, hence the term 'boosting'. One approach to correct for flux boosting follows from Bayes' theorem:

$$P(S_{\rm true}|S_{\rm obs},\sigma_{\rm obs}) \propto P(S_{\rm true})P(S_{\rm obs}|S_{\rm true},\sigma_{\rm obs}), \tag{2.1}$$

where $S_{\rm true}$ is the intrinsic source flux density, $S_{\rm obs}$ is the measured source flux density and $\sigma_{\rm obs}$ is the measured source uncertainty. If the source uncertainties are Gaussian then $P(S_{\rm obs}|S_{\rm true},\sigma_{\rm obs}) \propto e^{-(S_{\rm true}-S_{\rm obs})^2/2\sigma^2_{\rm obs}}$. Here $P(S_{\rm true})$ is the prior, which quantifies all previous knowledge that we might have about the distribution of flux densities in our sample.

To construct the prior we performed a set of simulations that reconstruct, as best as possible, our observing strategy. For each of the five fields in our study we first produced a mock SCUBA-2 map with 2 arcsec $\times$ 2 arcsec pixels by injecting sources into an area of blank sky matching the area surveyed in the SCUBA-2 CLS. The flux densities were drawn from a Schechter-type function of the form

$$\frac{dN}{dS} = \left(\frac{N_0}{S_0}\right)\left(\frac{S}{S_0}\right)^{-\gamma} e^{-S/S_0}. \tag{2.2}$$

We adopted parameters obtained by Casey et al. (2013) from a fit to the number counts in a roughly $0.1\,{\rm deg}^2$ portion of the COSMOS field, namely $N_0 = 3300\,{\rm deg}^{-2}$, $S_0 = 3.7\,{\rm mJy}$ and $\gamma = 1.4$. While Geach et al. (2017) also fit this model to their number counts, we found that the above values

were more consistent with our data as they predicted more bright sources. Positions were randomly selected to simulate Poisson statistics, with no clustering. The maps were convolved with a nominal SCUBA-2 beam with a FWHM of 14.8 arcsec and a negative bowl (from Geach et al. 2017). Gaussian noise was added followed by a second smoothing with the SCUBA-2 beam, which is the matched filter that optimizes point-source detection (see Chapin et al. 2011, Appendix A). The amplitude of the Gaussian noise is such that, after application of the matched filter, the resulting rms is equivalent to the rms achieved in each fields' actual map. We note that in practice the SCUBA-2 noise is not Gaussian and is correlated; however, the SCUBA-2 CLS areas were covered sufficiently uniformly that our method does not introduce significant errors.

To simulate the SMA follow-ups, we found all peaks in the map brighter than a certain cutoff, which was determined to be the faintest non-deboosted SCUBA-2 source targeted by our actual SMA observations in a given field. The mock SMA follow-ups were performed by creating 9 arcsec $\times$ 9 arcsec thumbnail images centred on a bright SCUBA-2 source's peak pixel; we chose 9 arcsec as a characteristic thumbnail size, since beyond this radius we no longer expect to be seeing the source/sources that contribute to the SCUBA-2 flux density we are following up. The thumbnail images have 0.1 arcsec pixel sizes and were smoothed by a 2.4-arcsec FWHM beam, which accurately reconstructed our actual SMA observations because most of the galaxies in our data are unresolved. Following Coppin et al. (2005, 2006), the distribution of pixel flux densities from all of the mock SMA observations is a good estimator for the prior, since it takes into account both resolution and selection effects present in our observations. For each of the five fields where we have data, we repeated our simulation a sufficient number of times to produce 100 deg^2, corresponding to over 70,000 sources brighter than 10 mJy. The parameters used in each of the five fields' simulations are summarized in Table 2.1.

Following Eq. 2.1, we constructed a posterior probability distribution for the intrinsic flux density of each source using priors from their respective fields. In Tables A.1–A.5 under the column S_{SMA} we report the deboosted flux density as the peak in the posterior probability distribution, and we give error bars representing 68 per cent confidence intervals. In Fig. 2.2 we show an example of this deboosting technique for a typical source, COSMOS07, which, according to our simulations, is expected to be 6.5 per cent fainter than indicated by our maps. Note that the error bars do not necessarily increase, but the signal always decreases so that the S/N always decreases.

Both LHN11 and LHN12, which had S/N values less than 4 but had

Table 2.1: Parameters describing our simulations, which we use to calculate the expected level of flux boosting in our measurements.

Field	S2 area [deg^2]	S2 noise [mJy]	S2 cutoff [mJy]
UDS	0.96	0.9	7.8
SSA22	0.28	1.2	6.7
COSMOS	2.22	1.6	7.2
LHN	0.28	1.1	8.1
EGS	0.32	1.2	9.8

good multiwavelength counterparts, had probability distribution peaks at zero flux density due to their low S/N. For these sources we report 68 per cent upper limits in the $S_{\rm SMA}$ column of Tables A.1–A.5. We also note that COSMOS22, which had a S/N value of 4.0, had a probability density function whose 68 per cent confidence interval overlapped with zero flux density, but we keep it as a detection.

Cases where a single bright SCUBA-2 source is resolved into two or more faint galaxies are more difficult to deboost. In our simulations we do not include any galaxy-galaxy interactions, clustering or lensing, and we only follow-up the SCUBA-2 sources brighter than a certain threshold, so we cannot use our approach to obtain deboosting fractions for those faint galaxies which contribute to single, bright SCUBA-2 peaks. However, should a bright SCUBA-2 source resolve into one bright SMG above our follow up threshold and one or more faint SMGs below our follow up threshold, our boosting correction would be applicable only to the bright SMG. We therefore define all faint galaxies to be those with flux densities 1 mJy less than the cutoff used to determine which SCUBA-2 sources were to be followed up by the SMA in our simulations in a given field. Galaxies LHN13a and LHN13b resolved completely from a SCUBA-2 peak and are considered faint, while galaxies COSMOS11b, LHN09b and LHN09c resolved from a SCUBA-2 peak along with a bright companion. We did not correct the measured flux densities for these SMGs, and we simply use the measured values throughout the paper; in the $S_{\rm SMA}$ column of Tables A.1–A.5, we report a value of N/A for these cases. We note that neglecting to deboost these faint sources will have no effect on the bright end of the number counts.

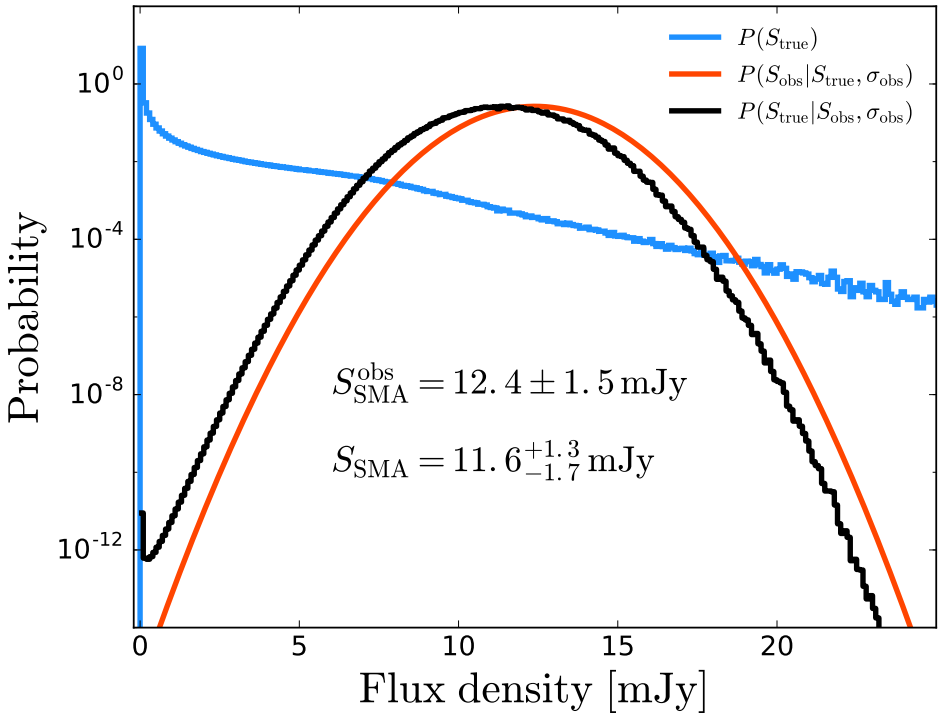

Figure 2.2: Probability distributions for the flux density of COSMOS07, a typical source in our data set. The blue curve is the prior, which is calculated by binning pixels resulting from simulating SCUBA-2 CLS fields and making small SMA thumbnail images centred on the brightest sources. The red curve shows the flux density of COSMOS07 measured from our data, where the uncertainty is assumed to be Gaussian. The black curve is the posterior probability distribution, which peaks at a slightly lower, deboosted flux density value due to the presence of many more faint galaxies in the simulated sky. The deboosted flux density uncertainties given represent a 68 per cent confidence interval about the peak.

2.3.2 Astrometry

The accuracy with which SCUBA-2 sources can be localized is well understood to be a function of observed S/N (assuming no multiplicity), and is approximated as (equation B22 in Ivison et al. 2007)

$$\Delta\alpha = \Delta\delta = 0.6 \text{ FWHM } [(\text{S/N})^2_{\text{obs}} - (2\beta + 4)]^{-1/2}, \tag{2.3}$$

where $\Delta\alpha$ is the uncertainty in right ascension (RA), $\Delta\delta$ is the uncertainty in declination (Dec), FWHM is the full-width half-maximum beamsize of SCUBA-2 and β is the local slope of the cumulative number count used as a prior to correct the observed flux densities for boosting. To examine the positional accuracy of our sample we computed the radial distance between our interferometrically-detected sources and those of the parent SCUBA-2 catalogue as a function of the detected S/N from Geach et al. (2017). For cases where multiple SMA/ALMA sources are detected, we simulated a simple (noiseless) SCUBA-2 image by convolving point sources at the SMA positions with a nominal SCUBA-2 beam with a FWHM of 14.8 arcsec (the best-fitting model from Geach et al. 2017, resulting from stacking 322 point sources of $> 5\sigma$ in the UDS map) and calculated the location of the peak intensity, which is then compared to the reported SCUBA-2 source position. We took into account offsets between the SMA and SCUBA-2 reference frames on a field-by-field basis by subtracting the mean difference in RA and Dec from each calculated offset.

In Fig. 2.3 we plot the radial separation of our SMA positions relative to the SCUBA-2 positions (except for the 12 sources where we did not detect a galaxy) as a function of detected S/N. Also shown are theoretical 68 per cent and 95 per cent contours, derived using Equation 2.3 with $\beta = 2.4$. To obtain the radial probability density we integrate $re^{-r^2/2\sigma^2}$, so 68 per cent and 95 per cent contours are are actually at 1.51σ and 2.50σ, respectively. Six sources lie above the 95 per cent contour, corresponding to about 10 per cent of the sources in our sample. While this may be more than expected, we note that in our simple simulations used to estimate the peak flux density position seen by SCUBA-2 using the SMA positions are priors, we did not include any SCUBA-2 noise. There also appears to be one outlier with a 9 arcsec offset. This outlier is LHN09, which we have identified as a triplet with one bright galaxy and two faint companions. The large offset seen here is directly attributed to LHN09a, the bright galaxy, and the peak of the flux density seen by SCUBA-2 in our simulation lies almost on top of it. Looking at Fig. B.1, we can see that LHN09 is a rather complicated system, with seven IR galaxies and five radio galaxies all within the SCUBA-2 beam. It

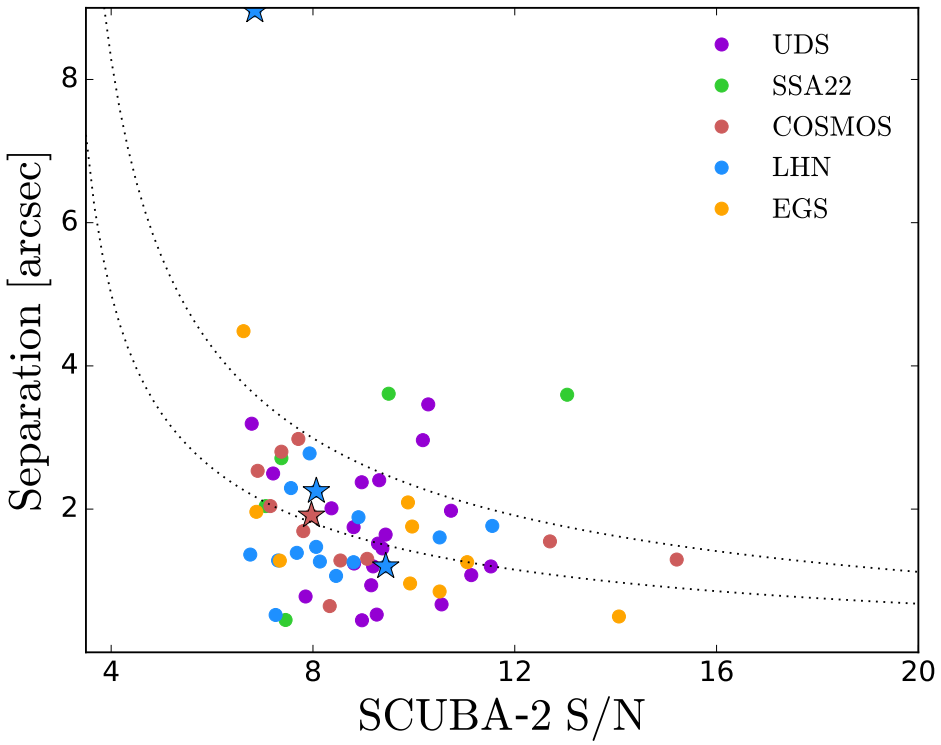

Figure 2.3: Radial offset of SMA-detected sources from their SCUBA-2 counterparts. Where multiple counterparts are detected we smooth the sources with the nominal SCUBA-2 beam and locate the peak flux density and compare this to the given SCUBA-2 position. These sources are highlighted in the figure by stars. Also shown are the expected 68 per cent and 95 per cent positional uncertainties as a functon of detected S/N for SCUBA-2.

is therefore possible that our SMA data has resolved out some of the flux density seen by SCUBA-2, which would in turn lead to the large offset we are seeing.

2.3.3 Flux density reliability

Next we compare the interferometric flux density observations to those from SCUBA-2 to check the reliability of the flux densities in our data set. We use the boosting-corrected flux densities reported by Geach et al. (2017) and our boosting-corrected flux densities. When comparing the cases where a singe-dish source is resolved into multiple components, we take into account the

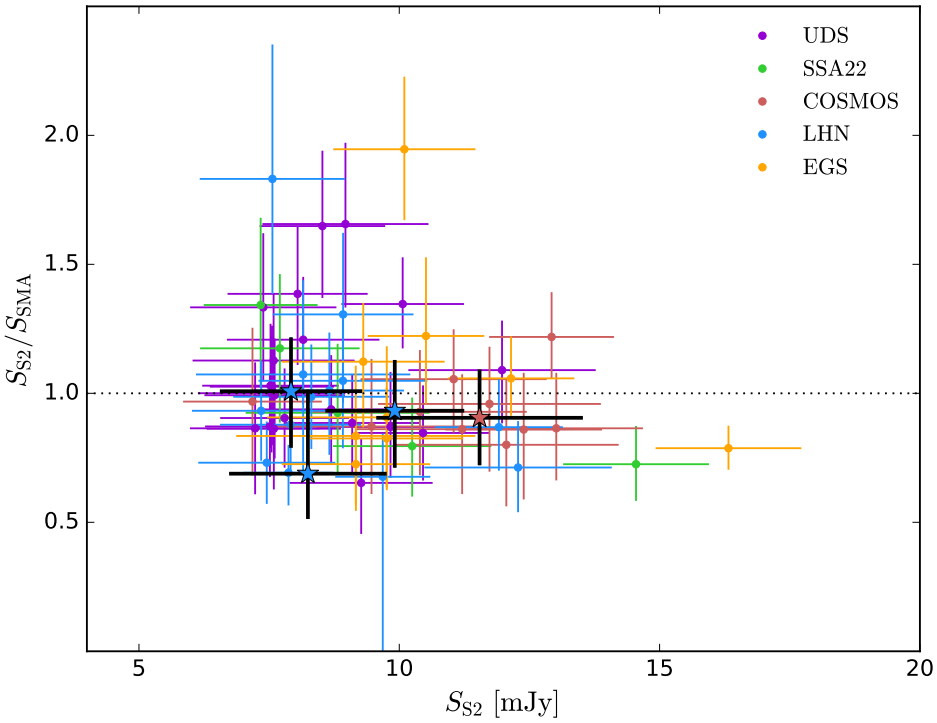

Figure 2.4: Comparison of the SCUBA-2 deboosted flux density from Geach et al. (2017) to the ratio of our SMA deboosted flux densities to each corresponding SCUBA-2 flux density. Where a single CLS source is resolved into multiple components, we have summed each components' flux density weighted by the SCUBA-2 beam response. These sources are shown as stars.

SCUBA-2 14.8 arcsec beamsize. To do this, for each component, we multiply the flux density by a 14.8-arcsec FWHM Gaussian, representing the SCUBA-2 beam, evaluated at the angular separation between the component and the location of the peak flux density seen in the SCUBA-2 map. Summing up these weighted flux densities is a better approximation to what was observed by SCUBA-2. The results are shown in Fig. 2.4, where we have plotted $S_{\rm S2}$ versus $S_{\rm SMA}/S_{\rm S2}$ and removed from our comparison the twelve sources where we only have upper limits on the flux density.

The mean value of the ratio $S_{\rm SMA}/S_{\rm S2}$ is 1.05 ± 0.03, where the uncertainty is the standard error of the mean. While this result does not provide evidence for missing flux from faint sources in our maps with detections, it is likely that there are faint sources below the the noise levels in our maps lacking detections – when we add these observations to the calculation of the mean value of $S_{\rm SMA}/S_{\rm S2}$ we get 0.87 ± 0.05.

2.3.4 Completeness

Here we discuss in detail the completeness of our observations with respect to the parent SCUBA-2 CLS survey. Since our targets were selected based on early CLS maps with higher noise, it is important to understand our sample in terms of the final, published maps. In addition, we have to decide how many sources from other experiments (i.e. Younger et al. 2007, 2009; Simpson et al. 2015) we wish to include in our sample, since they will affect our completeness.

The latter question is important because we have not specifically targeted any sources below the given flux density limit (which depends on the field); however, images from Younger et al. (2007, 2009) and Simpson et al. (2015) extend much deeper, and in several cases a faint source that would have been omitted from our study turned out to be bright enough to affect the bright end of the number counts when observed by the SMA or ALMA. Including sources like this could potentially bias our results, since our survey would then not really be 'blind', rendering the analysis much more difficult to interpret.

Our approach to this problem involves two steps. First, we incorporate into our catalogue all sources from Younger et al. (2007, 2009) and Simpson et al. (2015) that have SCUBA-2 deboosted flux densities greater than the faintest source we targeted in our observations in a given field (see Table 2.1, under the 'S2 thresh' column). These sources are included in Tables A.1–A.5, and we have used the numbering conventions given in their respective papers. There are seven sources from Younger et al. (2007), four sources

from Younger et al. (2009) and 16 sources from Simpson et al. (2015), for a total of 27 archival sources. We note that the flux densities from Younger et al. (2007, 2009) have not been corrected for flux boosting, so we use their direct measurements and give the deboosted flux densities under the $S_{\rm SMA}$ column as N/A; the flux densities from Simpson et al. (2015) have been corrected for flux boosting, which are given under the $S_{\rm ALMA}$ column, and we use these values for further analysis. We also include in our work the SMA observation of Orochi from Ikarashi et al. (2011), the gravitational lense in the UDS field. This brings the total number of interferometric samples in our analysis to 103.

Next, we calculate a completeness level for that field by dividing the total number of SCUBA-2 sources targeted in our sample by the total number of SCUBA-2 sources in the parent sample in a given flux density bin. We looked at bins above 8 mJy with widths of $\Delta S = 1$ mJy. In this way we are effectively treating the external sources as if we had targeted them ourselves, indroducing as little bias as possible, while still using all of the data. We can then use the calculated completeness values in each bin to correct for the missing sources introduced in the final, deeper CLS SCUBA-2 maps.

In the UDS field, we have targeted sources down to SCUBA-2-deboosted flux densities of 7.2 mJy. After introducing the sources from Simpson et al. (2015) with deboosted SCUBA-2 flux densities greater than 7.2 mJy, we find that our catalogue reaches a completeness of 96 per cent for $S > 8$ mJy, where the unobserved 4 per cent of sources are cases where a SCUBA-2 flux density was scattered to a higher value with the additional exposure time. At fainter flux densities our completeness falls below 80 per cent, which we deem to be too low to be used reliable, and in the brighter regime of $S > 9$ mJy we have 100 per cent completeness. A similar analysis performed for the ALMA sources observed by Simpson et al. (2015) resulted in completeness levels of 50 per cent for $S > 8$ mJy, 56 per cent for $S > 9$ mJy, and 73 per cent for $S > 10$ mJy, which shows that our observations offer a significant improvement in this field owing to the fact that our targets were selected from later versions of the CLS maps.

In the SSA22 field we have followed up 100 per cent of the sources with a deboosted SCUBA-2 flux density greater than 10 mJy. In this field there are no sources with SCUBA-2 deboosted flux densities between 9 and 10 mJy, and below 9 mJy our data do not cover enough sources to allow us to reliably estimate the number counts. Despite the fact that we have targeted five additional sources less than the 10 mJy level, two sources scattered up to about 8 mJy in the deeper SSA22 CLS map after our targets were selected, and so our completeness for $S > 8$ mJy is only 71 per cent.

In the COSMOS field, only about 50 per cent of the total area was mapped to a nominal depth of 1.6 mJy in the published CLS maps used in our study, and the remaining half is currently being completed (S2COSMOS: Simpson et al. in prep); our completeness calculation for this field is based on the current data available in Geach et al. (2017). We find that, with the addition of the observations from Younger et al. (2007, 2009) down to 7.1 mJy, our faintest target, we have completeness of 89 per cent for $S > 10$ mJy, and 100 per cent completeness for $S > 11$ mJy. Below 10 mJy our sample becomes very sparse. There are two sources with deboosted SCUBA-2 flux densities of 10.0 and 10.1 mJy that have not been observed with the SMA in our campaign, nor in the work of Younger et al. (2007, 2009), due to their low S/N in earlier SCUBA-2 and LABOCA maps.

We have fully probed the LHN field down to 7.5 mJy, achieving 100 per cent completeness. Below this we targeted one source whose corresponding deboosted SCUBA-2 flux density is 7.3 mJy, but we do not try to probe number counts this low.

Lastly, our sample does not include any EGS members below 9 mJy, while above 9 mJy we have resolved all of the available CLS sources, and thus every detection is statistically significant for estimating the counts in this field.

We now consider the completeness of our total data set. We have observed nearly all sources down to 10 mJy in these five cosmological fields, reaching a completeness level of 95 per cent for $S > 10$ mJy. As described above, there are two SCUBA-2 sources with deboosted flux densities of 10.0 and 10.1 mJy that have no interferometric data, both in the COSMOS field. When considering our full data set, these two sources comprise 5 per cent of the total number of sources with flux densities above 10 mJy. In Table 2.2 we summarize our completeness calculations for each field, for $S > 8$ mJy and $S > 10$ mJy.

2.4 Results and discussion

2.4.1 Number counts

We now estimate the cumulative number counts of our sample of interferometrically-detected SMGs. Our calculations are restricted to counts within the completeness regimes discussed above. The areas for each field are given in Geach et al. (2017) and are 0.96 deg^2 for the UDS field, 0.28 deg^2 for the SSA22 field, 2.22 deg^2 for the COSMOS field, 0.28 deg^2 for the LHN field and 0.32 deg^2 for the EGS field, totalling 4.06 deg^2 for our complete survey.

Table 2.2: Completeness levels calculated for each field in our study, as well as for the total data set.

Field	Completeness > 8 mJy	Completeness > 10 mJy
UDS	96%	100%
SSA22	71%	100%
COSMOS	54%	89%
LHN	100%	100%
EGS	N/A	100%
Total	77%	95%

We calculate the cumulative number count in bins of $\Delta S = 1$ mJy by simply counting the total number of sources $> S$ and dividing by the total area. To correct for the incompleteness due to the two COSMOS sources lacking SMA data in the $S > 10$ mJy bin, we first identify all sources in our catalogue that have a SCUBA-2 deboosted flux density within $\pm\, 0.5$ mJy of the missing sources' flux densities, and then we average over our corresponding SMA deboosted measurements. For the missing 10.0 mJy COSMOS source we get 10.2 mJy, and for the missing 10.1 mJy COSMOS source we get 10.5 mJy. These two values are then used for calculating the number counts.

For the twelve observations where only upper limits were obtained for the SMA counterparts we use the upper limit flux density as the deboosted SMA flux density; all 4σ upper limits we have measured constrain the flux densities of these sources to be less than 10 mJy, below the regime where we have good completeness, so we are not introducing any bias in the flux density region studied in this work by doing this. The source SSA22-04 is however an exception, where we have constrained the flux density to be less than 12.6 mJy but the corresponding SCUBA-2 flux density is 10.0 mJy. Since our SMA observations of this source have not been able to provide any further information, we adopt the same method used for the two missing COSMOS sources and use a flux density of 10.2 mJy for calculating the number counts. Lastly, for plotting purposes, we remove all repeated points, that is, points where there is no change in the cumulative number count in two adjacent bins because there are no sources between S and $S + \Delta S$.

The results for the cumulative number count are shown in Fig. 2.5. The error bars are calculated as 68 per cent confidence intervals from Poisson statistics (see Gehrels 1986). In addition, we show the CLS cumulative count results from Geach et al. (2017) for comparison. We have also shaded

the boundary marking the 100 per cent completeness of our sample.

We then compute the differential number counts in each field, following the same procedure as above. The results are shown in Fig. 2.5, beside our cumulative number counts and together with the CLS differential counts from Geach et al. (2017) and the region marking the boundary of 100 per cent completeness.

In Fig. 2.6 we show our cumulative and differential number counts for the UDS field alone compared to those derived by Simpson et al. (2015), along with the shaded region indicating our 100 per cent completeness limit. There seems to be a slight lack of sources at $S \gtrsim 10\,\mathrm{mJy}$ seen by Simpson et al. (2015), but this is probably due to incompleteness in their data; there are three SCUBA-2 sources (UDS03, UDS08 and UDS09) that were not targeted in their work as they did not appear to among the brightest 30 UDS sources in the earlier, shallower CLS maps used to design their follow-up ALMA programme. Also shown in Fig. 2.6 is the cumulative and differential count from the SCUBA-2 data in Geach et al. (2017). By including the three bright UDS sources to the number counts we find no strong evidence for diagreement between the single-dish measurements from Geach et al. (2017), the measurements from Simpson et al. (2015) and our work within the uncertainties.

Similar single dish counts were also obtained by the LESS survey (Weiß et al. 2009), which was a 0.35-deg^2 870-μm survey of the *Chandra* Deep Field South carried out with LABOCA, which has a FWHM of 19.2 arcsec. The LESS survey detected a total of 126 submm galaxies to a noise level of approximately 1.2 mJy. Following this, a high-resolution follow-up campaign was carried out by Hodge et al. (2013) using ALMA, and the number counts were presented by Karim et al. (2013). They found no sources brighter than about 9 mJy despite there being 12 LABOCA sources in this regime, implying a cut-off to possible FIR luminosities and star-formation rates.

We compare our results to these earlier works in Fig. 2.7, where on the top row we have plotted the cumulative and differential number counts from LESS and the CLS (i.e. two single dish submm surveys), and on the bottom row we have plotted the cumulative and differential number counts from Karim et al. (2013), Simpson et al. (2015) and our work (i.e. high angular resolution follow-up studies); the shaded region indicating where our data is no longer 100 per cent complete is shown as well. We see no evidence for a lack of high flux density sources, as hinted at by the results of Karim et al. (2013), and instead see the number count carrying on at a relatively constant slope to around 15 mJy. In this plot we have included the number counts from models of evolving star-forming galaxies, specifically the

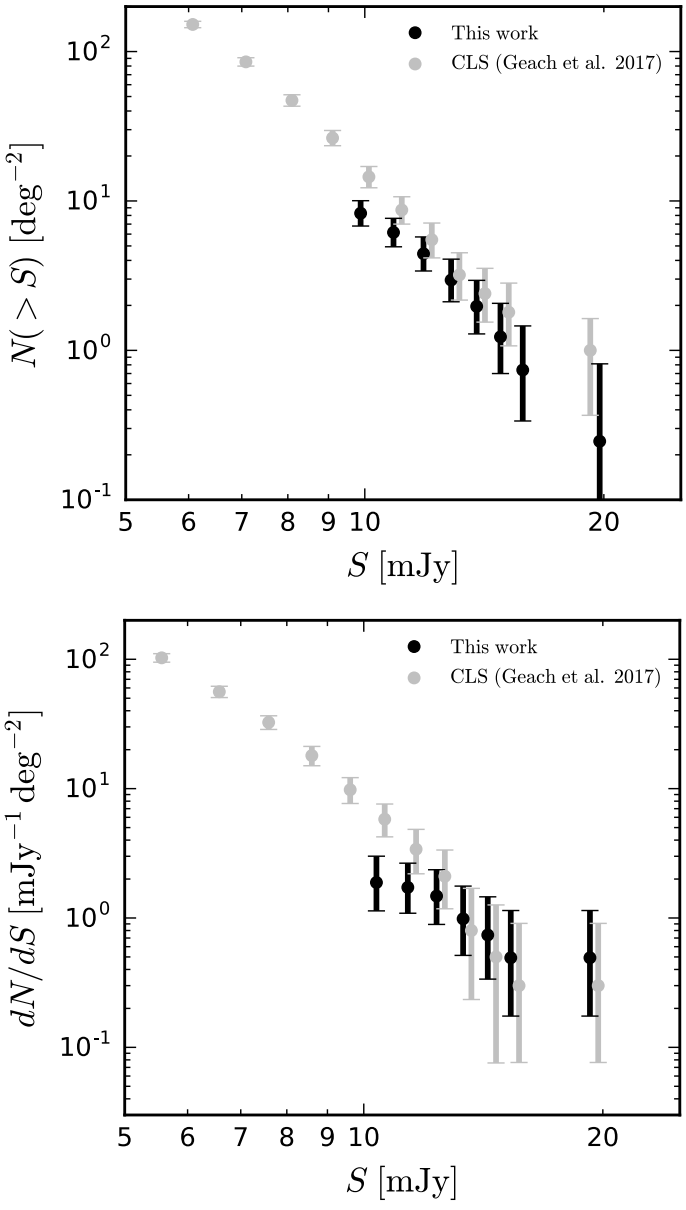

Figure 2.5: Cumulative (above) and differentia (below) number counts derived from our data set. The single dish results from the CLS (Geach et al. 2017) are shown for comparison. Values are slightly offset from each other in each bin for clarity. The shaded region marks where our data is no longer 100 per cent complete. An offset between our results of 2 to 20 per cent is seen in the cumulative count, although the points overlap within the uncertainties.

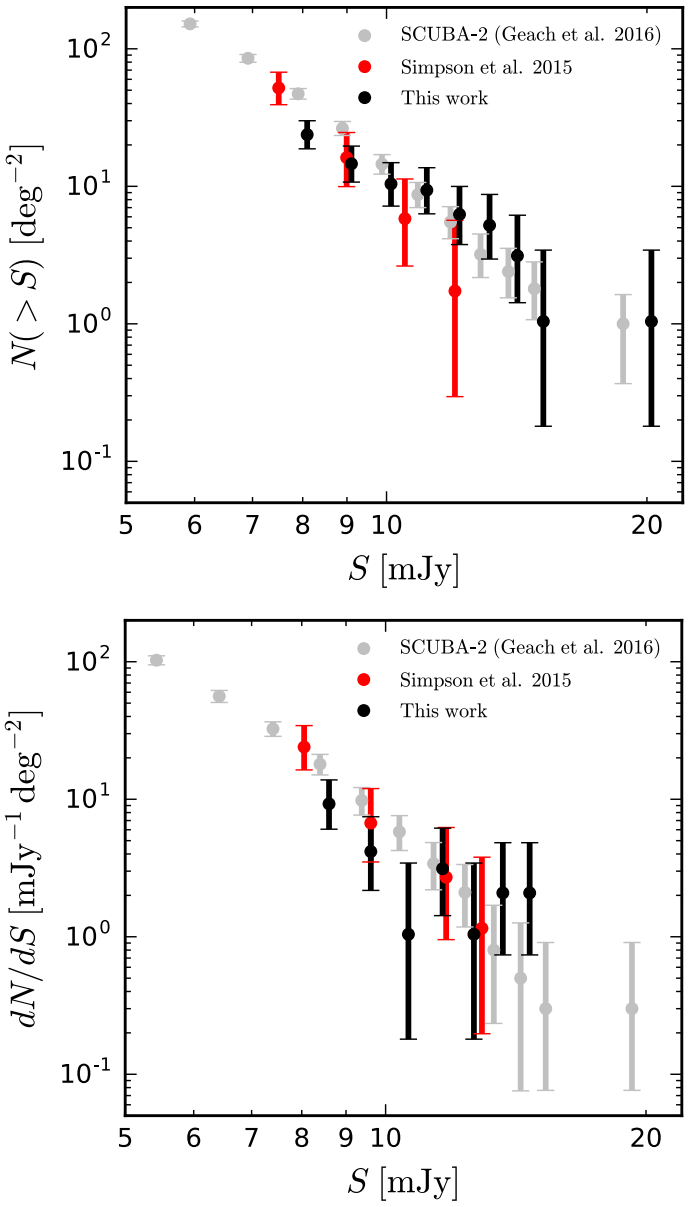

Figure 2.6: Cumulative (above) and differential (below) number count comparison for the UDS field. The restults from Simpson et al. (2015), derived from a smaller sample of the full parent CLS catalogue of the UDS field, are shown in red, alongside our more complete sample in black, where we have used only data from the UDS field as well. The results broadly agree, although we see evidence for less bright sources in the Simpson et al. (2015) sample. Also shown as the shaded region is where our data is not 100 per cent complete; our UDS data is 96 per cent complete for $S > 8$ mJy.

empirical model from Béthermin et al. (2012) and the GALFORM model from Lacey et al. (2016). While the model from Lacey et al. (2016) appears to be a better fit to our data, it is worth noting that the model from Béthermin et al. (2012) contains much less assumptions and no tuneable parameters (such as active galactic nuclei feedback and an adjustable initial mass function).

Lastly, we fit a power law to our differential count in order to quantitatively compare our results with these other works. We fit only points between 11 and 16 mJy, since our flux density coverage for smaller values is not 100 per cent complete, and beyond 16 mJy the differential number count begins to flatten, likely due to gravitational lensing not captured by a simple power law. Our model is of the form

$$\frac{dN}{dS} = N_0 S^{-\gamma}, \tag{2.4}$$

and we find best-fit parameters of $\gamma = 4.1 \pm 1.9$ and $N_0 = (0.4 \pm 1.8) \times 10^5\,\mathrm{mJy}^{-1}\,\mathrm{deg}^{-1}$. This best-fit curve is plotted alongside our data in Fig. 2.7. We then compute the χ^2 value between our model and the two data points between 11 and 16 mJy from Simpson et al. (2015), finding a value of 0.34. Taking the number of degrees of freedom to be 1, this corresponds to a p-value of 0.56. A similar analysis for the five data points (so 4 degrees of freedom) from Geach et al. (2017) between 11 and 16 mJy results in a χ^2 value of 3.99 and a p-value of 0.41. These p-values, being much greater than the commonly used threshold of 0.05, do not suggest that the differential measurements from Simpson et al. (2015) and Geach et al. (2017) differ significantly from our best-fit power law model within the flux density range of 11 to 16 mJy, although it is worth noting that we have not incorporated the uncertainty of the best-fit parameters in this analysis.

Even though this simple calculation shows that our results and those from the parent CLS sample are largely consistent, it should be noted that the two data sets are entirely correlated, being observations of the exact same galaxies. Thus any differences at all in the counts, even if they are within the Poisson errors, still carry importance. In particular, the cumulative distribution in Fig. 2.5 suggests a systematic offset of a few up to about 20 per cent for all flux density bins.

2.4.2 Multiplicity

The importance of galaxy interactions and mergers for the intense star-formation rates observed in many submm galaxies is a hotly debated topic.

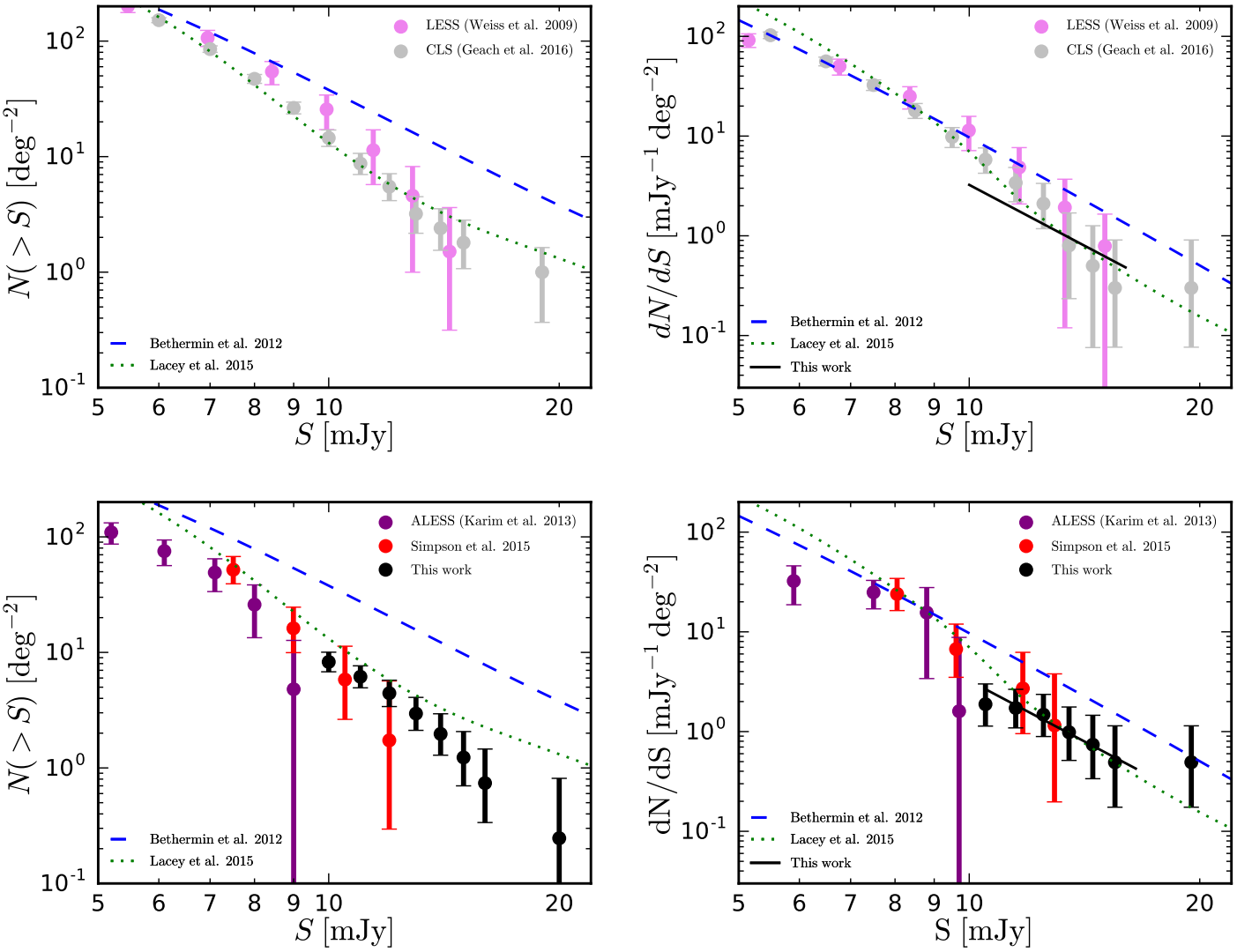

Figure 2.7: Cumulative and differential number counts for the two large single dish submm surveys LESS (Weiß et al. 2009) and CLS (Geach et al. 2017) on the top row. On the bottom row we show cumulative and differential number counts from Karim et al. (2013) and Simpson et al. (2015), interferometric follow-up studies of the LESS and CLS surveys, respectfully, shown along with our SMA results and the shaded region indicating where our data is no longer 100 per cent complete. Also shown are the models of Béthermin et al. (2012) and Lacey et al. (2016). The black solid line shows the best-fit power to our differential distribution between 11 and 16 mJy.

Here we discuss the multiplicity seen in our large sample of bright, 850-μm-selected galaxies at a resolution of about 2 arcsec, and contrast our observations with previous works.

There is first the question of how to precisely define a multiple; with enough sensitivity, due to the steep rise in number counts at fainter flux densities, one could start to detect very faint background sources that are not in fact associated. Our observations, being sensitive only down to about 6 mJy, would not suffer from this problem, but, for example, Lambas et al. (2012) defined multipes by their flux ratio, and pairs with brightest to second-brightest ratios less than 3 were considered multples, since this value provides a reasonable cut-off for finding single dish sources whose flux densities have been seriously affected. Our observations are not able to detect ratios as high as 3 but we have probed the regime of ratios less than 2, where single dish flux densities are the most seriously affected; in the following discussion we use this as a working definition for multiplicity in our sample.

In the UDS field, we found that none of our 23 observed SCUBA-2 sources break up into two components, while the ALMA follow-up results of Simpson et al. (2015) reported 18 single dish sources breaking up into multiple components in 30 observations, a fraction of 0.60 ± 0.14, where the uncertainty is calculated as the square root of the number of multiples divided by the sample size. It is hard to directly compare these two results for several reasons. First, Simpson et al. (2015) targeted most of the $S > 10$ mJy sources in this field, while we have followed-up those in the fainter 8–10 mJy regime, and we might expect brighter SCUBA-2 sources to have a higher chance of being composed of multiple galaxies. Second, the typical rms level obtained in the ALMA images was about 0.2 mJy, compared to our SMA images, which have about 1.5 mJy of noise. For example, in cases where a single bright SCUBA-2 source is composed of one bright galaxy and several fainter ($\lesssim 5$ mJy) galaxies below the detection limit of the SMA, we might expect to see one detection with the SMA and multiple detections with ALMA. Third, the synthesized beam of the ALMA pointings was about 0.35 arcsec, much smaller than the 2.4 arcsec synthesized beam we achieved with the SMA. We could therefore still be blending sources together, but only if they are genuinely close on the sky – Simpson et al. (2015) found only two cases with equally bright galaxies separated by less than the SMA beamsize.

In the COSMOS field we found that one SCUBA-2 source resolved into two components. Including AzTEC11 from Younger et al. (2009), also a multiple, we obtain a multiplicity fraction of 0.07 ± 0.05 out of 27 SMA observations. We note that the full catalogues published in Younger et al.

(2007, 2009) contained two multiples, one of which is not included in our observations since its SCUBA-2 counterpart was not detected in the CLS.

In the LHN field we found that, of the 18 SCUBA-2 sources followed-up, two break up into two galaxies, and one breaks up into three galaxies, which is a multiplicity fraction of 0.17 ± 0.10. This field represents the highest such fraction in our sample; however, it still does not approach the multiplicity fraction seen in the Simpson et al. (2015) sample. The remaining fields, SSA22 and EGS, did not show any multiple-galaxy SCUBA-2 sources.

The fact that we did not robustly detect any sources in twelve of our pointings may in several cases be attributed to faint multiples being washed out by the noise level in our SMA observations. Using more sensitive ALMA observations, Simpson et al. (2015) found four cases of bright, 7–11 mJy SCUBA-2 sources resolving into multiple < 5 mJy sources, which would not be detected in most of our SMA pointings. It is thus plausible to attribute some of our null-detections to cases where the SCUBA-2 blended source is composed of multiple faint sources that are lost in the noise; however, we must be careful with this interpretation as there are instances where the flux density threshold in our SMA maps is greater than the flux density of the SCUBA-2 source we are trying to detect. In these cases we cannot claim evidence for detecting multiplicity. Specifically, UDS14, UDS15, SSA22-03, COSMOS06, COSMOS17, LHN11 and LHN12 each have SMA flux density limits less than their observed SCUBA-2 counterpart flux densities, and so may be composed of multiple galaxies below our 4σ limit, whereas for SSA22-04, SSA22-07, SSA22-09, COSMOS23 and COSMOS25 we are not able to say anything about the galaxies contributing to the SCUBA-2 flux density. Under the interpretation that undetected sources constrainted by our SMA observations to be fainter than their SCUBA-2 measurements are in fact multiples, we actually have observed seven more of these systems.

This interpretation would change the multiplicity fraction in the COSMOS field to 0.15 ± 0.07, and the multiplicity fraction in the LHN field to 0.28 ± 0.12, while in the SSA22 field we can calculate a fraction of 0.11 ± 0.11. In the UDS field, in order to properly incorporate the ALMA observations (taking into account the difference in sensitivity compared to the SMA) we include multiples from Simpson et al. (2015) where two or more sources have flux densities greater than 6 mJy or where all multiples are less than 6 mJy, which assumes a mean 1.5 mJy noise level and a 4σ cut. This includes four multiples: UDS156.0 and UDS156.1; UDS57.0 and UDS57.1; UDS286.0, UDS286.1, UDS286.2 and UDS286.3; and UDS199.0 and UDS199.1. Then, incorporating the two non-detections from our SMA observations, we find a multiplicity fraction of 0.15 ± 0.06, which agrees well with the other fields.

The GOODS-N field, a smaller, 0.07 deg^2 part of the CLS, has also been probed with the SMA. In particular, Barger et al. (2014) provided a compilation of 28 SMA observations of known SCUBA-2 sources, 11 of which had flux densities brighter than 8 mJy. The mean noise obtained by these SMA observations was 1.1 mJy. In this work, after application of a 4σ cut, none of these brighter sources were seen to break up into multiple components, but three fainter SCUBA-2 sources did break up. While this sample is not sufficiently complete to calculate number counts, Chen et al. (2013) pointed out that the single-dish counts were not significantly affeced by multiplicity.

Considering our entire catalogue, we have a total of 16 multiples in 102 observations (removing the gravitational lens Orochi), which results in a multiplicity fraction of 0.16 ± 0.04. It is worth noting once more the assumptions we have made to get to this number. First, we have assumed that undetected sources with flux density constraints less than what was observed by SCUBA-2 are multiples, but this might not be true if an intrinsically faint SCUBA-2 source were to lie on a rather large positive noise peak. Second, we have assumed that there are no multiples where we have not been able to gain any interferometric information due to large amounts of noise, which might not be true in particular for SSA22-04, a 10 mJy SCUBA-2 source which could potentially be resolved into two similarly bright galaxies detectable by the SMA.

Our data therefore suggest that about 15 per cent of single dish submm sources brighter than 10 mJy will be seen as multiple SMGs with brightest to second-brightest flux density ratios less than 2 when viewed with an angular resolution of 2.4 arcsec. This multiplicity fraction can be thought of as depending on three parameters: the minimum flux densities targeted, the sensitivity of the interferometric observations, and the angular resolution of the interferometric observations. In targeting brighter sources, we expect to observe more multiples (when strong lensing is not considered), and in addition, more sensitive instruments with better angular resolution, like ALMA, should also observe more multiples.

The question of wheather the multiplicity seen in our SMA images correspond directly to galaxy mergers is difficult to address with our data. First, we note that the physical scale being probed by the SMA's resolution, namely 2.4 arcsec, at a fiducual redshift of 2 is about 20 kpc, which is around the same separation seen with major-mergers in the local Universe (e.g. Lambas et al. 2012, who examined a set of about 2000 galaxy pairs at $z < 0.1$). On the other hand, it has been suggested that line-of-sight projections could account for a significant fraction of the multiplicity seen in bright SMGs (Cowley et al. 2015), although larger sample sizes will be

required to better understand this fraction over larger scales. But the fact that we hardly see any multiples may be useful for detecting galaxy clusters in formation. Under the assumption that these multiples are in fact physically associated, merging galaxies, one could reasonably expect that the few instances of multiplicity where both galaxies are equally bright are massive galaxy cluster cores in the midst of formation, being such rare events. However, the sensitivity of our SMA observations only allows us to detect up to two galaxies per single SCUBA-2 source (there is no way to divide a 12 mJy source into three parts brighter than 6 mJy, the typical noise level in our data – the two faint companions to LHN09 technically fall below our S/N threshold of 4), which may be too few to be the progenitor of today's massive galaxy clusters. Nonetheless, the fact that we do not observe very many equally bright pairs may help future work constrain massive cluster formation.

2.4.3 Density of extremely luminous galaxies

Our sample of galaxies represent some of the most luminous and intensely star-forming sites in the Universe. The SEDs of SMGs are well described by a modified blackbody function (e.g., Dale and Helou 2002; Blain et al. 2004):

$$S(\nu, T_{\rm d}, C, z) = C\,(\nu(1+z))^{\beta}\,\frac{(\nu(1+z))^3}{e^{h\nu(1+z)/k_B T_{\rm d}}-1}, \tag{2.5}$$

which depends on a dust temperature $T_{\rm d}$, the redshift z, a normalization constant C. The spectral emissivity index β, which is the power law that 'modifies' the blackbody, is usually fixed at 2 based on physical arguments (Draine 2011). We can estimate the IR luminosity for a typical 10 mJy source in our sample by setting $\beta = 2$, $z = 2$, $T_{\rm d} = 30$ K and normalizing to 10 mJy at 860 μm then integrating this model from 8 to 1000 μm (which is the definition of the IR luminosity). This calclation results in $6 \times 10^{12}\,{\rm L}_{\odot}$, and this can be converted to a SFR using the relationship from Kennicutt (1998) modified for a Chabrier IMF (Chabrier 2003) (i.e. ${\rm SFR}[{\rm M}_{\odot}\,{\rm yr}^{-1}] = 9.5\times10^{-11}\,{\rm L}_{\rm IR}/{\rm L}_{\odot}$) to get $550\,{\rm M}_{\odot}\,{\rm yr}^{-1}$.

Using the above result we can recast our number counts in terms of intrinsic SFRs. Since we see a surface density of galaxies brighter than 10 mJy of $8^{+2}_{-1}\,{\rm deg}^{-2}$, this is a good approximation for the number of galaxies with SFRs $\gtrsim 500\,{\rm M}_{\odot}\,{\rm yr}^{-1}$. Here we are assuming that none of our sources are being gravitationally lensed, which would reduce their intrinsic SFRs; we will address the fraction of gravitaionally lensed galaxies in our sample

in future work. Assuming all of our sources lie between $z = 2$ and $z = 3$ and using the cosmological parameters from Planck Collaboration XIII (2016), this implies a likely volume density of $660^{+140}_{-120}\,\mathrm{Gpc}^{-3}$. With our data we are not able to determine the number of nearby foreground galaxies that do not actually possess such high SFRs or that do not fall into the redshift range used for our volume calculation, but such a correction should not be larger than a factor of a few.

2.5 Summary

Using the SMA we have followed-up 75 of the brightest SCUBA-2 CLS sources spread across $4\,\mathrm{deg}^2$ in five fields. We have also included in our analysis 28 archival SMA and ALMA observations of similar nature to bring our total sample size to 103. The synthesized beam of our observations was on average 2.4 arcsec FWHM and the noise 1.5 mJy as calculated from the primary beam-corrected images, sufficient to resolve the majority of the SMGs contributing to the flux density peaks seen by the SCUBA-2 instrument. Altogether, we detected 66 SMGs above 4σ, and saw three examples of a single SCUBA-2 peak breaking up into two or more SMGs. We also found that ten of our pointings did not detect any SMGs, which may result from a SCUBA-2 peak breaking up into two or more SMGs fainter than our 4σ detection limit, which is on average 6 mJy. We found four more sources with 3σ SMA peaks coincident with IR/radio data, two of which are counterparts to a brighter SMA galaxy while the other two are individual galaxies, which we include in our work to bring the number of galaxy detections to 70.

We simulated SCUBA-2 maps and SMA follow-up pointings using the same selection criteria as for our observations in order to estimate and correct for flux boosting in our measurements. Upon applying these corrections, we found that the posterior probability distributions of two sources peaked at 0 mJy, so we can only constrain 68 per cent upper limits on their flux densities. We tested our positional accuracy by calculating the radial distance from the peak flux density positions in our SMA images to those in the CLS maps, finding the spread to be consistent with the expected spread given the S/N values. We also compared our deboosted flux density measurements to the deboosted flux density measurements published in the CLS, and found the mean ratio to be $S_{\mathrm{S2}}/S_{\mathrm{SMA}} = 1.05 \pm 0.03$.

Assessing completeness, our sample consists of 95 per cent of the sources with $S > 10$ mJy with respect to the reference fields in the CLS, and we

calculate the number counts for this regime. We compare our number counts to what was found in our parent sample, finding general agreement; however, we do find a systematic offset between 2 and 20 per cent. We also compare our counts to those from Simpson et al. (2015), who followed-up most of the bright sources in the UDS field of the CLS with ALMA, and we show that the two estimations are in agreement.

While multiplicity is evidently not uncommon in most of the bright single-dish sources, the effects appear not to severely steepen the bright end of the number counts. We estimate an upper limit of 15 per cent to the multiplicity fraction of single dish submm sources brighter than approximately 10 mJy, defined as groups of SMGs with brightest to second-brightest flux density ratios less than 2. Instead, the most common situation involves bright single dish submm sources resolving into one slightly less bright SMG and several much fainter ones with much larger flux density ratios, which only slightly lowers previous estimates of the number of bright SMGs.

Lastly we calculate the surface density of galaxies with SFRs greater than approximately $500\,\mathrm{M_\odot\,yr^{-1}}$ to be $8^{+2}_{-1}\,\mathrm{deg^{-2}}$, and assuming all redshifts are between 2 and 3, a volume density of $660^{+140}_{-120}\,\mathrm{Gpc^{-3}}$.

Chapter 3

Conclusion

SMGs have proven to contain a wealth of information regarding the high redshift Universe; since their discovery in the late 1990s, they have continuously been a prolific area of research. It has become very clear that SMGs represent a population of galaxies in the very early Universe, with a redshift distribution peaking between 2 and 2.5, which translates to a time when the Universe was only about 3 billion years old. They have incredibly bright IR luminosities, which average to about $L_{IR} \approx 10^{12} L_{\odot}$. Since L_{IR} is expected to be directly proportional to the SFR, SMGs must also be some of the most intensely star-forming sources of their epoch – values well over $1000\,M_{\odot}\,yr^{-1}$ have been observed.

New telescopes with high resolution and improved sensitivity are beginning to break up some of the brightest submm sources into multiple SMGs. This has been important when considering number counts and resolving the CIB. The improvements in resolution are important when considering theoretical models and numerical simulations of SMG formation. The sheer number of ultraluminous SMGs seen on the sky is very difficult to reproduce. Major mergers require more inter-halo collision in the early Universe than permitted by theoretical calculations, while standard galactic evolution through gas accretion has been shown through simulations to be incapable of reaching large enough luminosities. If it turns out that the majority of SMGs break up into smaller, less luminous components, models and simulations will not have to duplicate such extreme scenarios.

There remain many unanswered questions; this is still a highly active field of research. Some of the most pressing issues include determining whether or not SMGs represent a common stage of galaxy evolution, revealing the physical mechanisms behind their incredible luminosities, and developing a comprehensive theory to describe the formation of SMGs – are mergers the primary drivers behind their development, or does the answer lie closer to the classic view of galaxy formation through accretion? Answering these questions will be crucial towards developing a better understanding of the nature and evolution of the Universe.

Bibliography

A. J. Barger, W.-H. Wang, L. L. Cowie, F. N. Owen, C.-C. Chen, and J. P. Williams. Precise Identifications of Submillimeter Galaxies: Measuring the History of Massive Star-forming Galaxies to z > 5. *Astrophysical Journal*, 761:89, December 2012. doi: 10.1088/0004-637X/761/2/89.

A. J. Barger, L. L. Cowie, C.-C. Chen, F. N. Owen, W.-H. Wang, C. M. Casey, N. Lee, D. B. Sanders, and J. P. Williams. Is There a Maximum Star Formation Rate in High-redshift Galaxies? *Astrophysical Journal*, 784:9, March 2014. doi: 10.1088/0004-637X/784/1/9.

C. M. Baugh, C. G. Lacey, C. S. Frenk, G. L. Granato, L. Silva, A. Bressan, A. J. Benson, and S. Cole. Can the faint submillimetre galaxies be explained in the Λ cold dark matter model? *Monthly Notices of the Royal Astronomical Society*, 356:1191–1200, January 2005. doi: 10.1111/j.1365-2966.2004.08553.x.

F. Bertoldi, C. Carilli, M. Aravena, E. Schinnerer, H. Voss, V. Smolcic, K. Jahnke, N. Scoville, A. Blain, K. M. Menten, D. Lutz, M. Brusa, Y. Taniguchi, P. Capak, B. Mobasher, S. Lilly, D. Thompson, H. Aussel, E. Kreysa, G. Hasinger, J. Aguirre, J. Schlaerth, and A. Koekemoer. COSBO: The MAMBO 1.2 Millimeter Imaging Survey of the COSMOS Field. *Astrophysical Journal Supplement*, 172:132–149, September 2007. doi: 10.1086/520511.

M. Béthermin, E. Daddi, G. Magdis, M. T. Sargent, Y. Hezaveh, D. Elbaz, D. Le Borgne, J. Mullaney, M. Pannella, V. Buat, V. Charmandaris, G. Lagache, and D. Scott. A Unified Empirical Model for Infrared Galaxy Counts Based on the Observed Physical Evolution of Distant Galaxies. *Astrophysical Journal Letters*, 757:L23, October 2012. doi: 10.1088/2041-8205/757/2/L23.

A. D. Biggs, R. J. Ivison, E. Ibar, J. L. Wardlow, H. Dannerbauer, I. Smail, F. Walter, A. Weiß, S. C. Chapman, K. E. K. Coppin, C. De Breuck, M. Dickinson, K. K. Knudsen, V. Mainieri, K. Menten, and C. Papovich.

The LABOCA survey of the Extended Chandra Deep Field-South - radio and mid-infrared counterparts to submillimetre galaxies. *Monthly Notices of the Royal Astronomical Society*, 413:2314–2338, June 2011. doi: 10.1111/j.1365-2966.2010.18132.x.

A. W. Blain, I. Smail, R. J. Ivison, and J.-P. Kneib. The history of star formation in dusty galaxies. *Monthly Notices of the Royal Astronomical Society*, 302:632–648, February 1999. doi: 10.1046/j.1365-8711.1999.02178.x.

A. W. Blain, I. Smail, R. J. Ivison, J.-P. Kneib, and D. T. Frayer. Submillimeter galaxies. *Physics Reports*, 369:111–176, October 2002. doi: 10.1016/S0370-1573(02)00134-5.

A. W. Blain, S. C. Chapman, I. Smail, and R. Ivison. Accurate Spectral Energy Distributions and Selection Effects for High-Redshift Dusty Galaxies: A New Hot Population to Discover with the Spitzer Space Telescope? *Astrophysical Journal*, 611:52–58, August 2004. doi: 10.1086/422026.

M. Casali, A. Adamson, C. Alves de Oliveira, O. Almaini, K. Burch, T. Chuter, J. Elliot, M. Folger, S. Foucaud, N. Hambly, M. Hastie, D. Henry, P. Hirst, M. Irwin, D. Ives, A. Lawrence, K. Laidlaw, D. Lee, J. Lewis, D. Lunney, S. McLay, D. Montgomery, A. Pickup, M. Read, N. Rees, I. Robson, K. Sekiguchi, A. Vick, S. Warren, and B. Woodward. The UKIRT wide-field camera. *Astronomy and Astrophysics*, 467: 777–784, May 2007. doi: 10.1051/0004-6361:20066514.

C. M. Casey, C.-C. Chen, L. L. Cowie, A. J. Barger, P. Capak, O. Ilbert, M. Koss, N. Lee, E. Le Floc'h, D. B. Sanders, and J. P. Williams. Characterization of SCUBA-2 450 μm and 850 μm selected galaxies in the COSMOS field. *Monthly Notices of the Royal Astronomical Society*, 436: 1919–1954, December 2013. doi: 10.1093/mnras/stt1673.

G. Chabrier. Galactic Stellar and Substellar Initial Mass Function. *Publications of the Astronomical Society of Japan*, 115:763–795, July 2003. doi: 10.1086/376392.

E. L. Chapin, S. C. Chapman, K. E. Coppin, M. J. Devlin, J. S. Dunlop, T. R. Greve, M. Halpern, M. F. Hasselfield, D. H. Hughes, R. J. Ivison, G. Marsden, L. Moncelsi, C. B. Netterfield, E. Pascale, D. Scott, I. Smail, M. Viero, F. Walter, A. Weiss, and P. van der Werf. A joint analysis of BLAST 250-500 μm and LABOCA 870 μm observations in the Extended Chandra Deep Field-South. *Monthly Notices of the Royal*

Astronomical Society, 411:505–549, February 2011. doi: 10.1111/j.1365-2966.2010.17697.x.

S. C. Chapman, A. W. Blain, I. Smail, and R. J. Ivison. A Redshift Survey of the Submillimeter Galaxy Population. *Astrophysical Journal*, 622:772–796, April 2005. doi: 10.1086/428082.

C.-C. Chen, L. L. Cowie, A. J. Barger, C. M. Casey, N. Lee, D. B. Sanders, W.-H. Wang, and J. P. Williams. Resolving the Cosmic Far-infrared Background at 450 and 850 μm with SCUBA-2. *Astrophysical Journal*, 776: 131, October 2013. doi: 10.1088/0004-637X/776/2/131.

C.-C. Chen, I. Smail, A. M. Swinbank, J. M. Simpson, C.-J. Ma, D. M. Alexander, A. D. Biggs, W. N. Brandt, S. C. Chapman, K. E. K. Coppin, A. L. R. Danielson, H. Dannerbauer, A. C. Edge, T. R. Greve, R. J. Ivison, A. Karim, K. M. Menten, E. Schinnerer, F. Walter, J. L. Wardlow, A. Weiß, and P. P. van der Werf. An ALMA Survey of Submillimeter Galaxies in the Extended Chandra Deep Field South: Near-infrared Morphologies and Stellar Sizes. *Astrophysical Journal*, 799:194, February 2015. doi: 10.1088/0004-637X/799/2/194.

C.-C. Chen, I. Smail, R. J. Ivison, V. Arumugam, O. Almaini, C. J. Conselice, J. E. Geach, W. G. Hartley, C.-J. Ma, A. Mortlock, C. Simpson, J. M. Simpson, A. M. Swinbank, I. Aretxaga, A. Blain, S. C. Chapman, J. S. Dunlop, D. Farrah, M. Halpern, M. J. Michałowski, P. van der Werf, A. Wilkinson, and J. A. Zavala. The SCUBA-2 Cosmology Legacy Survey: Multiwavelength Counterparts to 10^3 Submillimeter Galaxies in the UKIDSS-UDS Field. *Astrophysical Journal*, 820:82, April 2016. doi: 10.3847/0004-637X/820/2/82.

K. Coppin, M. Halpern, D. Scott, C. Borys, and S. Chapman. An 850-μm SCUBA map of the Groth Strip and reliable source extraction. *Monthly Notices of the Royal Astronomical Society*, 357:1022–1028, March 2005. doi: 10.1111/j.1365-2966.2005.08723.x.

K. Coppin, E. L. Chapin, A. M. J. Mortier, S. E. Scott, C. Borys, J. S. Dunlop, M. Halpern, D. H. Hughes, A. Pope, D. Scott, S. Serjeant, J. Wagg, D. M. Alexander, O. Almaini, I. Aretxaga, T. Babbedge, P. N. Best, A. Blain, S. Chapman, D. L. Clements, M. Crawford, L. Dunne, S. A. Eales, A. C. Edge, D. Farrah, E. Gaztañaga, W. K. Gear, G. L. Granato, T. R. Greve, M. Fox, R. J. Ivison, M. J. Jarvis, T. Jenness, C. Lacey, K. Lepage, R. G. Mann, G. Marsden, A. Martinez-Sansigre, S. Oliver,

M. J. Page, J. A. Peacock, C. P. Pearson, W. J. Percival, R. S. Priddey, S. Rawlings, M. Rowan-Robinson, R. S. Savage, M. Seigar, K. Sekiguchi, L. Silva, C. Simpson, I. Smail, J. A. Stevens, T. Takagi, M. Vaccari, E. van Kampen, and C. J. Willott. The SCUBA Half-Degree Extragalactic Survey - II. Submillimetre maps, catalogue and number counts. *Monthly Notices of the Royal Astronomical Society*, 372:1621–1652, November 2006. doi: 10.1111/j.1365-2966.2006.10961.x.

W. I. Cowley, C. G. Lacey, C. M. Baugh, and S. Cole. Simulated observations of sub-millimetre galaxies: the impact of single-dish resolution and field variance. *Monthly Notices of the Royal Astronomical Society*, 446: 1784–1798, January 2015. doi: 10.1093/mnras/stu2179.

D. A. Dale and G. Helou. The Infrared Spectral Energy Distribution of Normal Star-forming Galaxies: Calibration at Far-Infrared and Submillimeter Wavelengths. *Astrophysical Journal*, 576:159–168, September 2002. doi: 10.1086/341632.

R. Davé, K. Finlator, B. D. Oppenheimer, M. Fardal, N. Katz, D. Kereš, and D. H. Weinberg. The nature of submillimetre galaxies in cosmological hydrodynamic simulations. *Monthly Notices of the Royal Astronomical Society*, 404:1355–1368, May 2010. doi: 10.1111/j.1365-2966.2010.16395.x.

J. M. Dickey and F. J. Lockman. H I in the Galaxy. *Annual Review of Astronomy and Astrophysics*, 28:215–261, 1990. doi: 10.1146/annurev.aa.28.090190.001243.

B. T. Draine. *Physics of the Interstellar and Intergalactic Medium*. 2011.

H. Engel, L. J. Tacconi, R. I. Davies, R. Neri, I. Smail, S. C. Chapman, R. Genzel, P. Cox, T. R. Greve, R. J. Ivison, A. Blain, F. Bertoldi, and A. Omont. Most Submillimeter Galaxies are Major Mergers. *Astrophysical Journal*, 724:233–243, November 2010. doi: 10.1088/0004-637X/724/1/233.

J. E. Geach, J. S. Dunlop, M. Halpern, I. Smail, P. van der Werf, D. M. Alexander, O. Almaini, I. Aretxaga, V. Arumugam, V. Asboth, M. Banerji, J. Beanlands, P. N. Best, A. W. Blain, M. Birkinshaw, E. L. Chapin, S. C. Chapman, C.-C. Chen, A. Chrysostomou, C. Clarke, D. L. Clements, C. Conselice, K. E. K. Coppin, W. I. Cowley, A. L. R. Danielson, S. Eales, A. C. Edge, D. Farrah, A. Gibb, C. M. Harrison, N. K. Hine, D. Hughes, R. J. Ivison, M. Jarvis, T. Jenness, S. F. Jones, A. Karim,

M. Koprowski, K. K. Knudsen, C. G. Lacey, T. Mackenzie, G. Marsden, K. McAlpine, R. McMahon, R. Meijerink, M. J. Michałowski, S. J. Oliver, M. J. Page, J. A. Peacock, D. Rigopoulou, E. I. Robson, I. Roseboom, K. Rotermund, D. Scott, S. Serjeant, C. Simpson, J. M. Simpson, D. J. B. Smith, M. Spaans, F. Stanley, J. A. Stevens, A. M. Swinbank, T. Targett, A. P. Thomson, E. Valiante, D. A. Wake, T. M. A. Webb, C. Willott, J. A. Zavala, and M. Zemcov. The SCUBA-2 Cosmology Legacy Survey: 850 μm maps, catalogues and number counts. *Monthly Notices of the Royal Astronomical Society*, 465:1789–1806, February 2017. doi: 10.1093/mnras/stw2721.

N. Gehrels. Confidence limits for small numbers of events in astrophysical data. *Astrophysical Journal*, 303:336–346, April 1986. doi: 10.1086/164079.

R. Genzel, A. J. Baker, L. J. Tacconi, D. Lutz, P. Cox, S. Guilloteau, and A. Omont. Spatially Resolved Millimeter Interferometry of SMM J02399-0136: AVery Massive Galaxy at z = 2.8. *Astrophysical Journal*, 584: 633–642, February 2003. doi: 10.1086/345718.

T. R. Greve, R. J. Ivison, F. Bertoldi, J. A. Stevens, J. S. Dunlop, D. Lutz, and C. L. Carilli. A 1200-μm MAMBO survey of ELAISN2 and the Lockman Hole - I. Maps, sources and number counts. *Monthly Notices of the Royal Astronomical Society*, 354:779–797, November 2004. doi: 10.1111/j.1365-2966.2004.08235.x.

M. J. Griffin, A. Abergel, A. Abreu, P. A. R. Ade, P. André, J.-L. Augueres, T. Babbedge, Y. Bae, T. Baillie, J.-P. Baluteau, M. J. Barlow, G. Bendo, D. Benielli, J. J. Bock, P. Bonhomme, D. Brisbin, C. Brockley-Blatt, M. Caldwell, C. Cara, N. Castro-Rodriguez, R. Cerulli, P. Chanial, S. Chen, E. Clark, D. L. Clements, L. Clerc, J. Coker, D. Communal, L. Conversi, P. Cox, D. Crumb, C. Cunningham, F. Daly, G. R. Davis, P. de Antoni, J. Delderfield, N. Devin, A. di Giorgio, I. Didschuns, K. Dohlen, M. Donati, A. Dowell, C. D. Dowell, L. Duband, L. Dumaye, R. J. Emery, M. Ferlet, D. Ferrand, J. Fontignie, M. Fox, A. Franceschini, M. Frerking, T. Fulton, J. Garcia, R. Gastaud, W. K. Gear, J. Glenn, A. Goizel, D. K. Griffin, T. Grundy, S. Guest, L. Guillemet, P. C. Hargrave, M. Harwit, P. Hastings, E. Hatziminaoglou, M. Herman, B. Hinde, V. Hristov, M. Huang, P. Imhof, K. J. Isaak, U. Israelsson, R. J. Ivison, D. Jennings, B. Kiernan, K. J. King, A. E. Lange, W. Latter, G. Laurent, P. Laurent, S. J. Leeks, E. Lellouch, L. Levenson, B. Li, J. Li, J. Lilien-

thal, T. Lim, S. J. Liu, N. Lu, S. Madden, G. Mainetti, P. Marliani, D. McKay, K. Mercier, S. Molinari, H. Morris, H. Moseley, J. Mulder, M. Mur, D. A. Naylor, H. Nguyen, B. O'Halloran, S. Oliver, G. Olofsson, H.-G. Olofsson, R. Orfei, M. J. Page, I. Pain, P. Panuzzo, A. Papageorgiou, G. Parks, P. Parr-Burman, A. Pearce, C. Pearson, I. Pérez-Fournon, F. Pinsard, G. Pisano, J. Podosek, M. Pohlen, E. T. Polehampton, D. Pouliquen, D. Rigopoulou, D. Rizzo, I. G. Roseboom, H. Roussel, M. Rowan-Robinson, B. Rownd, P. Saraceno, M. Sauvage, R. Savage, G. Savini, E. Sawyer, C. Scharmberg, D. Schmitt, N. Schneider, B. Schulz, A. Schwartz, R. Shafer, D. L. Shupe, B. Sibthorpe, S. Sidher, A. Smith, A. J. Smith, D. Smith, L. Spencer, B. Stobie, R. Sudiwala, K. Sukhatme, C. Surace, J. A. Stevens, B. M. Swinyard, M. Trichas, T. Tourette, H. Triou, S. Tseng, C. Tucker, A. Turner, M. Vaccari, I. Valtchanov, L. Vigroux, E. Virique, G. Voellmer, H. Walker, R. Ward, T. Waskett, M. Weilert, R. Wesson, G. J. White, N. Whitehouse, C. D. Wilson, B. Winter, A. L. Woodcraft, G. S. Wright, C. K. Xu, A. Zavagno, M. Zemcov, L. Zhang, and E. Zonca. The Herschel-SPIRE instrument and its in-flight performance. *Astronomy and Astrophysics*, 518:L3, July 2010. doi: 10.1051/0004-6361/201014519.

E. J. Groth, J. A. Kristian, R. Lynds, E. J. O'Neil, Jr., R. Balsano, J. Rhodes, and WFPC-1 IDT. A Survey with the HST. In *American Astronomical Society Meeting Abstracts*, volume 26 of *Bulletin of the American Astronomical Society*, page 1403, December 1994.

C. Gruppioni, F. Pozzi, G. Rodighiero, I. Delvecchio, S. Berta, L. Pozzetti, G. Zamorani, P. Andreani, A. Cimatti, O. Ilbert, E. Le Floc'h, D. Lutz, B. Magnelli, L. Marchetti, P. Monaco, R. Nordon, S. Oliver, P. Popesso, L. Riguccini, I. Roseboom, D. J. Rosario, M. Sargent, M. Vaccari, B. Altieri, H. Aussel, A. Bongiovanni, J. Cepa, E. Daddi, H. Domínguez-Sánchez, D. Elbaz, N. Förster Schreiber, R. Genzel, A. Iribarrem, M. Magliocchetti, R. Maiolino, A. Poglitsch, A. Pérez García, M. Sanchez-Portal, E. Sturm, L. Tacconi, I. Valtchanov, A. Amblard, V. Arumugam, M. Bethermin, J. Bock, A. Boselli, V. Buat, D. Burgarella, N. Castro-Rodríguez, A. Cava, P. Chanial, D. L. Clements, A. Conley, A. Cooray, C. D. Dowell, E. Dwek, S. Eales, A. Franceschini, J. Glenn, M. Griffin, E. Hatziminaoglou, E. Ibar, K. Isaak, R. J. Ivison, G. Lagache, L. Levenson, N. Lu, S. Madden, B. Maffei, G. Mainetti, H. T. Nguyen, B. O'Halloran, M. J. Page, P. Panuzzo, A. Papageorgiou, C. P. Pearson, I. Pérez-Fournon, M. Pohlen, D. Rigopoulou, M. Rowan-Robinson,

B. Schulz, D. Scott, N. Seymour, D. L. Shupe, A. J. Smith, J. A. Stevens, M. Symeonidis, M. Trichas, K. E. Tugwell, L. Vigroux, L. Wang, G. Wright, C. K. Xu, M. Zemcov, S. Bardelli, M. Carollo, T. Contini, O. Le Févre, S. Lilly, V. Mainieri, A. Renzini, M. Scodeggio, and E. Zucca. The Herschel PEP/HerMES luminosity function - I. Probing the evolution of PACS selected Galaxies to z $\simeq$ 4. *Monthly Notices of the Royal Astronomical Society*, 432:23–52, June 2013. doi: 10.1093/mnras/stt308.

S. Guilloteau, J. Delannoy, D. Downes, A. Greve, M. Guelin, R. Lucas, D. Morris, S. J. E. Radford, J. Wink, J. Cernicharo, T. Forveille, S. Garcia-Burillo, R. Neri, J. Blondel, A. Perrigourad, D. Plathner, and M. Torres. The IRAM interferometer on Plateau de Bure. *Astronomy and Astrophysics*, 262:624–633, September 1992.

M. G. Hauser, R. G. Arendt, T. Kelsall, E. Dwek, N. Odegard, J. L. Weiland, H. T. Freudenreich, W. T. Reach, R. F. Silverberg, S. H. Moseley, Y. C. Pei, P. Lubin, J. C. Mather, R. A. Shafer, G. F. Smoot, R. Weiss, D. T. Wilkinson, and E. L. Wright. The COBE Diffuse Infrared Background Experiment Search for the Cosmic Infrared Background. I. Limits and Detections. *Astrophysical Journal*, 508:25–43, November 1998. doi: 10.1086/306379.

P. T. P. Ho, J. M. Moran, and K. Y. Lo. The Submillimeter Array. *Astrophysical Journal Letters*, 616:L1–L6, November 2004. doi: 10.1086/423245.

J. A. Hodge, A. Karim, I. Smail, A. M. Swinbank, F. Walter, A. D. Biggs, R. J. Ivison, A. Weiss, D. M. Alexander, F. Bertoldi, W. N. Brandt, S. C. Chapman, K. E. K. Coppin, P. Cox, A. L. R. Danielson, H. Dannerbauer, C. De Breuck, R. Decarli, A. C. Edge, T. R. Greve, K. K. Knudsen, K. M. Menten, H.-W. Rix, E. Schinnerer, J. M. Simpson, J. L. Wardlow, and P. van der Werf. An ALMA Survey of Submillimeter Galaxies in the Extended Chandra Deep Field South: Source Catalog and Multiplicity. *Astrophysical Journal*, 768:91, May 2013. doi: 10.1088/0004-637X/768/1/91.

W. S. Holland, E. I. Robson, W. K. Gear, C. R. Cunningham, J. F. Lightfoot, T. Jenness, R. J. Ivison, J. A. Stevens, P. A. R. Ade, M. J. Griffin, W. D. Duncan, J. A. Murphy, and D. A. Naylor. SCUBA: a common-user submillimetre camera operating on the James Clerk Maxwell Telescope. *Monthly Notices of the Royal Astronomical Society*, 303:659–672, March 1999. doi: 10.1046/j.1365-8711.1999.02111.x.

W. S. Holland, D. Bintley, E. L. Chapin, A. Chrysostomou, G. R. Davis, J. T. Dempsey, W. D. Duncan, M. Fich, P. Friberg, M. Halpern, K. D. Irwin, T. Jenness, B. D. Kelly, M. J. MacIntosh, E. I. Robson, D. Scott, P. A. R. Ade, E. Atad-Ettedgui, D. S. Berry, S. C. Craig, X. Gao, A. G. Gibb, G. C. Hilton, M. I. Hollister, J. B. Kycia, D. W. Lunney, H. McGregor, D. Montgomery, W. Parkes, R. P. J. Tilanus, J. N. Ullom, C. A. Walther, A. J. Walton, A. L. Woodcraft, M. Amiri, D. Atkinson, B. Burger, T. Chuter, I. M. Coulson, W. B. Doriese, C. Dunare, F. Economou, M. D. Niemack, H. A. L. Parsons, C. D. Reintsema, B. Sibthorpe, I. Smail, R. Sudiwala, and H. S. Thomas. SCUBA-2: the 10 000 pixel bolometer camera on the James Clerk Maxwell Telescope. *Monthly Notices of the Royal Astronomical Society*, 430:2513–2533, April 2013. doi: 10.1093/mnras/sts612.

S. Ikarashi, K. Kohno, J. E. Aguirre, I. Aretxaga, V. Arumugam, J. E. Austermann, J. J. Bock, C. M. Bradford, M. Cirasuolo, L. Earle, H. Ezawa, H. Furusawa, J. Furusawa, J. Glenn, B. Hatsukade, D. H. Hughes, D. Iono, R. J. Ivison, S. Johnson, J. Kamenetzky, R. Kawabe, R. Lupu, P. Maloney, H. Matsuhara, P. D. Mauskopf, K. Motohara, E. J. Murphy, K. Nakajima, K. Nakanishi, B. J. Naylor, H. T. Nguyen, T. A. Perera, K. S. Scott, K. Shimasaku, T. Takagi, T. Takata, Y. Tamura, K. Tanaka, T. Tsukagoshi, D. J. Wilner, G. W. Wilson, M. S. Yun, and J. Zmuidzinas. Detection of an ultrabright submillimetre galaxy in the Subaru/XMM-Newton Deep Field using AzTEC/ASTE. *Monthly Notices of the Royal Astronomical Society*, 415:3081–3096, August 2011. doi: 10.1111/j.1365-2966.2011.18918.x.

D. Iono, A. B. Peck, A. Pope, C. Borys, D. Scott, D. J. Wilner, M. Gurwell, P. T. P. Ho, M. S. Yun, S. Matsushita, G. R. Petitpas, J. S. Dunlop, M. Elvis, A. Blain, and E. Le Floc'h. Interferometric 890 μm Images of High-Redshift Submillimeter Galaxies. *Astrophysical Journal Letters*, 640:L1–L4, March 2006. doi: 10.1086/503290.

R. J. Ivison, T. R. Greve, I. Smail, J. S. Dunlop, N. D. Roche, S. E. Scott, M. J. Page, J. A. Stevens, O. Almaini, A. W. Blain, C. J. Willott, M. J. Fox, D. G. Gilbank, S. Serjeant, and D. H. Hughes. Deep radio imaging of the SCUBA 8-mJy survey fields: submillimetre source identifications and redshift distribution. *Monthly Notices of the Royal Astronomical Society*, 337:1–25, November 2002. doi: 10.1046/j.1365-8711.2002.05900.x.

R. J. Ivison, T. R. Greve, J. S. Dunlop, J. A. Peacock, E. Egami, I. Smail,

E. Ibar, E. van Kampen, I. Aretxaga, T. Babbedge, A. D. Biggs, A. W. Blain, S. C. Chapman, D. L. Clements, K. Coppin, D. Farrah, M. Halpern, D. H. Hughes, M. J. Jarvis, T. Jenness, J. R. Jones, A. M. J. Mortier, S. Oliver, C. Papovich, P. G. Pérez-González, A. Pope, S. Rawlings, G. H. Rieke, M. Rowan-Robinson, R. S. Savage, D. Scott, M. Seigar, S. Serjeant, C. Simpson, J. A. Stevens, M. Vaccari, J. Wagg, and C. J. Willott. The SCUBA HAlf Degree Extragalactic Survey - III. Identification of radio and mid-infrared counterparts to submillimetre galaxies. *Monthly Notices of the Royal Astronomical Society*, 380:199–228, September 2007. doi: 10.1111/j.1365-2966.2007.12044.x.

A. Karim, A. M. Swinbank, J. A. Hodge, I. R. Smail, F. Walter, A. D. Biggs, J. M. Simpson, A. L. R. Danielson, D. M. Alexander, F. Bertoldi, C. de Breuck, S. C. Chapman, K. E. K. Coppin, H. Dannerbauer, A. C. Edge, T. R. Greve, R. J. Ivison, K. K. Knudsen, K. M. Menten, E. Schinnerer, J. L. Wardlow, A. Weiß, and P. van der Werf. An ALMA survey of submillimetre galaxies in the Extended Chandra Deep Field South: high-resolution 870 μm source counts. *Monthly Notices of the Royal Astronomical Society*, 432:2–9, June 2013. doi: 10.1093/mnras/stt196.

R. C. Kennicutt, Jr. Star Formation in Galaxies Along the Hubble Sequence. *Annual Review of Astronomy and Astrophysics*, 36:189–232, 1998. doi: 10.1146/annurev.astro.36.1.189.

A. Kirkpatrick, A. Pope, D. M. Alexander, V. Charmandaris, E. Daddi, M. Dickinson, D. Elbaz, J. Gabor, H. S. Hwang, R. Ivison, J. Mullaney, M. Pannella, D. Scott, B. Altieri, H. Aussel, F. Bournaud, V. Buat, D. Coia, H. Dannerbauer, K. Dasyra, J. Kartaltepe, R. Leiton, L. Lin, G. Magdis, B. Magnelli, G. Morrison, P. Popesso, and I. Valtchanov. GOODS-Herschel: Impact of Active Galactic Nuclei and Star Formation Activity on Infrared Spectral Energy Distributions at High Redshift. *Astrophysical Journal*, 759:139, November 2012. doi: 10.1088/0004-637X/759/2/139.

M. P. Koprowski, J. S. Dunlop, M. J. Michałowski, M. Cirasuolo, and R. A. A. Bowler. A reassessment of the redshift distribution and physical properties of luminous (sub-)millimetre galaxies. *Monthly Notices of the Royal Astronomical Society*, 444:117–128, October 2014. doi: 10.1093/mnras/stu1402.

M. P. Koprowski, J. S. Dunlop, M. J. Michałowski, I. Roseboom, J. E. Geach, M. Cirasuolo, I. Aretxaga, R. A. A. Bowler, M. Banerji, N. Bourne,

K. E. K. Coppin, S. Chapman, D. H. Hughes, T. Jenness, R. J. McLure, M. Symeonidis, and P. v. d. Werf. The SCUBA-2 Cosmology Legacy Survey: galaxies in the deep 850 μm survey, and the star-forming 'main sequence'. *Monthly Notices of the Royal Astronomical Society*, 458:4321–4344, June 2016. doi: 10.1093/mnras/stw564.

M. P. Koprowski, J. S. Dunlop, M. J. Michałowski, K. E. K. Coppin, J. E. Geach, R. J. McLure, D. Scott, and P. P. van der Werf. The evolving far-IR galaxy luminosity function and dust-obscured star-formation rate density out to z˜5. *ArXiv e-prints*, June 2017.

C. G. Lacey, C. M. Baugh, C. S. Frenk, A. J. Benson, R. G. Bower, S. Cole, V. Gonzalez-Perez, J. C. Helly, C. D. P. Lagos, and P. D. Mitchell. A unified multiwavelength model of galaxy formation. *Monthly Notices of the Royal Astronomical Society*, 462:3854–3911, November 2016. doi: 10.1093/mnras/stw1888.

D. G. Lambas, S. Alonso, V. Mesa, and A. L. O'Mill. Galaxy interactions. I. Major and minor mergers. *Astronomy and Astrophysics*, 539:A45, March 2012. doi: 10.1051/0004-6361/201117900.

A. Lawrence, S. J. Warren, O. Almaini, A. C. Edge, N. C. Hambly, R. F. Jameson, P. Lucas, M. Casali, A. Adamson, S. Dye, J. P. Emerson, S. Foucaud, P. Hewett, P. Hirst, S. T. Hodgkin, M. J. Irwin, N. Lodieu, R. G. McMahon, C. Simpson, I. Smail, D. Mortlock, and M. Folger. The UKIRT Infrared Deep Sky Survey (UKIDSS). *Monthly Notices of the Royal Astronomical Society*, 379:1599–1617, August 2007. doi: 10.1111/j.1365-2966.2007.12040.x.

H. M. Lee, S. J. Kim, M. Im, H. Matsuhara, S. Oyabu, T. Wada, T. Nakagawa, J. Ko, H. J. Shim, M. G. Lee, N. Hwang, T. Takagi, and C. Pearson. North Ecliptic Pole Wide Field Survey of AKARI: Survey Strategy and Data Characteristics. *Publications of the Astronomical Society of Japan*, 61:375–385, February 2009. doi: 10.1093/pasj/61.2.375.

B. D. Lehmer, W. N. Brandt, D. M. Alexander, F. E. Bauer, D. P. Schneider, P. Tozzi, J. Bergeron, G. P. Garmire, R. Giacconi, R. Gilli, G. Hasinger, A. E. Hornschemeier, A. M. Koekemoer, V. Mainieri, T. Miyaji, M. Nonino, P. Rosati, J. D. Silverman, G. Szokoly, and C. Vignali. The Extended Chandra Deep Field-South Survey: Chandra Point-Source Catalogs. *Astrophysical Journal Supplement*, 161:21–40, November 2005. doi: 10.1086/444590.

S. J. Lilly, L. L. Cowie, and J. P. Gardner. A deep imaging and spectroscopic survey of faint galaxies. *Astrophysical Journal*, 369:79–105, March 1991. doi: 10.1086/169740.

S. J. Lilly, S. A. Eales, W. K. P. Gear, F. Hammer, O. Le Fèvre, D. Crampton, J. R. Bond, and L. Dunne. The Canada-United Kingdom Deep Submillimeter Survey. II. First Identifications, Redshifts, and Implications for Galaxy Evolution. *Astrophysical Journal*, 518:641–655, June 1999. doi: 10.1086/307310.

T. P. MacKenzie, D. Scott, M. Bianconi, D. L. Clements, H. A. Dole, I. Flores-Cacho, D. Guery, R. Kneissl, G. Lagache, F. R. Marleau, L. Montier, N. P. H. Nesvadba, E. Pointecouteau, and G. Soucail. SCUBA-2 follow-up of Herschel-SPIRE observed Planck overdensities. *Monthly Notices of the Royal Astronomical Society*, 468:4006–4017, July 2017. doi: 10.1093/mnras/stx512.

B. Magnelli, D. Lutz, P. Santini, A. Saintonge, S. Berta, M. Albrecht, B. Altieri, P. Andreani, H. Aussel, F. Bertoldi, M. Béthermin, A. Bongiovanni, P. Capak, S. Chapman, J. Cepa, A. Cimatti, A. Cooray, E. Daddi, A. L. R. Danielson, H. Dannerbauer, J. S. Dunlop, D. Elbaz, D. Farrah, N. M. Förster Schreiber, R. Genzel, H. S. Hwang, E. Ibar, R. J. Ivison, E. Le Floc'h, G. Magdis, R. Maiolino, R. Nordon, S. J. Oliver, A. Pérez García, A. Poglitsch, P. Popesso, F. Pozzi, L. Riguccini, G. Rodighiero, D. Rosario, I. Roseboom, M. Salvato, M. Sanchez-Portal, D. Scott, I. Smail, E. Sturm, A. M. Swinbank, L. J. Tacconi, I. Valtchanov, L. Wang, and S. Wuyts. A Herschel view of the far-infrared properties of submillimetre galaxies. *Astronomy and Astrophysics*, 539:A155, March 2012. doi: 10.1051/0004-6361/201118312.

B. Magnelli, P. Popesso, S. Berta, F. Pozzi, D. Elbaz, D. Lutz, M. Dickinson, B. Altieri, P. Andreani, H. Aussel, M. Béthermin, A. Bongiovanni, J. Cepa, V. Charmandaris, R.-R. Chary, A. Cimatti, E. Daddi, N. M. Förster Schreiber, R. Genzel, C. Gruppioni, M. Harwit, H. S. Hwang, R. J. Ivison, G. Magdis, R. Maiolino, E. Murphy, R. Nordon, M. Pannella, A. Pérez García, A. Poglitsch, D. Rosario, M. Sanchez-Portal, P. Santini, D. Scott, E. Sturm, L. J. Tacconi, and I. Valtchanov. The deepest Herschel-PACS far-infrared survey: number counts and infrared luminosity functions from combined PEP/GOODS-H observations. *Astronomy and Astrophysics*, 553:A132, May 2013. doi: 10.1051/0004-6361/201321371.

J. C. Mather, D. J. Fixsen, and R. A. Shafer. Design for the COBE far-infrared absolute spectrophotometer (FIRAS). In M. S. Scholl, editor, *Infrared Spaceborne Remote Sensing*, volume 2019 of *Proceedings of the SPIE*, pages 168–179, October 1993.

M. J. Michałowski, J. S. Dunlop, M. P. Koprowski, M. Cirasuolo, J. E. Geach, R. A. A. Bowler, A. Mortlock, K. I. Caputi, I. Aretxaga, V. Arumugam, C.-C. Chen, R. J. McLure, M. Birkinshaw, N. Bourne, D. Farrah, E. Ibar, P. van der Werf, and M. Zemcov. The SCUBA-2 Cosmology Legacy Survey: the nature of bright submm galaxies from 2 deg2 of 850-μm imaging. *Monthly Notices of the Royal Astronomical Society*, 469: 492–515, July 2017. doi: 10.1093/mnras/stx861.

O. Miettinen, M. Novak, V. Smolčić, E. Schinnerer, M. Sargent, E. J. Murphy, M. Aravena, M. Bondi, C. L. Carilli, A. Karim, M. Salvato, and G. Zamorani. (Sub)millimetre interferometric imaging of a sample of COSMOS/AzTEC submillimetre galaxies. II. The spatial extent of the radio-emitting regions. *Astronomy and Astrophysics*, 584:A32, December 2015. doi: 10.1051/0004-6361/201526589.

D. Narayanan, C. C. Hayward, T. J. Cox, L. Hernquist, P. Jonsson, J. D. Younger, and B. Groves. The formation of high-redshift submillimetre galaxies. *Monthly Notices of the Royal Astronomical Society*, 401:1613–1619, January 2010. doi: 10.1111/j.1365-2966.2009.15790.x.

D. Narayanan, M. Turk, R. Feldmann, T. Robitaille, P. Hopkins, R. Thompson, C. Hayward, D. Ball, C.-A. Faucher-Giguère, and D. Kereš. The formation of submillimetre-bright galaxies from gas infall over a billion years. *Nature*, 525:496–499, September 2015. doi: 10.1038/nature15383.

G. Neugebauer, H. J. Habing, R. van Duinen, H. H. Aumann, B. Baud, C. A. Beichman, D. A. Beintema, N. Boggess, P. E. Clegg, T. de Jong, J. P. Emerson, T. N. Gautier, F. C. Gillett, S. Harris, M. G. Hauser, J. R. Houck, R. E. Jennings, F. J. Low, P. L. Marsden, G. Miley, F. M. Olnon, S. R. Pottasch, E. Raimond, M. Rowan-Robinson, B. T. Soifer, R. G. Walker, P. R. Wesselius, and E. Young. The Infrared Astronomical Satellite (IRAS) mission. *Astrophysical Journal Letters*, 278:L1–L6, March 1984. doi: 10.1086/184209.

S. Noll, D. Burgarella, E. Giovannoli, V. Buat, D. Marcillac, and J. C. Muñoz-Mateos. Analysis of galaxy spectral energy distributions from far-UV to far-IR with CIGALE: studying a SINGS test sample. *Astronomy*

and Astrophysics, 507:1793–1813, December 2009. doi: 10.1051/0004-6361/200912497.

S. J. Oliver, L. Wang, A. J. Smith, B. Altieri, A. Amblard, V. Arumugam, R. Auld, H. Aussel, T. Babbedge, A. Blain, J. Bock, A. Boselli, V. Buat, D. Burgarella, N. Castro-Rodríguez, A. Cava, P. Chanial, D. L. Clements, A. Conley, L. Conversi, A. Cooray, C. D. Dowell, E. Dwek, S. Eales, D. Elbaz, M. Fox, A. Franceschini, W. Gear, J. Glenn, M. Griffin, M. Halpern, E. Hatziminaoglou, E. Ibar, K. Isaak, R. J. Ivison, G. Lagache, L. Levenson, N. Lu, S. Madden, B. Maffei, G. Mainetti, L. Marchetti, K. Mitchell-Wynne, A. M. J. Mortier, H. T. Nguyen, B. O'Halloran, A. Omont, M. J. Page, P. Panuzzo, A. Papageorgiou, C. P. Pearson, I. Pérez-Fournon, M. Pohlen, J. I. Rawlings, G. Raymond, D. Rigopoulou, D. Rizzo, I. G. Roseboom, M. Rowan-Robinson, M. Sánchez Portal, R. Savage, B. Schulz, D. Scott, N. Seymour, D. L. Shupe, J. A. Stevens, M. Symeonidis, M. Trichas, K. E. Tugwell, M. Vaccari, E. Valiante, I. Valtchanov, J. D. Vieira, L. Vigroux, R. Ward, G. Wright, C. K. Xu, and M. Zemcov. HerMES: SPIRE galaxy number counts at 250, 350, and 500 μm. *Astronomy and Astrophysics*, 518:L21, July 2010. doi: 10.1051/0004-6361/201014697.

E. Pascale, P. A. R. Ade, J. J. Bock, E. L. Chapin, J. Chung, M. J. Devlin, S. Dicker, M. Griffin, J. O. Gundersen, M. Halpern, P. C. Hargrave, D. H. Hughes, J. Klein, C. J. MacTavish, G. Marsden, P. G. Martin, T. G. Martin, P. Mauskopf, C. B. Netterfield, L. Olmi, G. Patanchon, M. Rex, D. Scott, C. Semisch, N. Thomas, M. D. P. Truch, C. Tucker, G. S. Tucker, M. P. Viero, and D. V. Wiebe. The Balloon-borne Large Aperture Submillimeter Telescope: BLAST. *Astrophysical Journal*, 681:400-414, July 2008. doi: 10.1086/588541.

Planck Collaboration XIII. *Planck* 2015 results. XIII. Cosmological parameters. *Astronomy and Astrophysics*, 594:A13, 2016. doi: 10.1051/0004-6361/201525830.

N. Rangwala, P. R. Maloney, J. Glenn, C. D. Wilson, A. Rykala, K. Isaak, M. Baes, G. J. Bendo, A. Boselli, C. M. Bradford, D. L. Clements, A. Cooray, T. Fulton, P. Imhof, J. Kamenetzky, S. C. Madden, E. Mentuch, N. Sacchi, M. Sauvage, M. R. P. Schirm, M. W. L. Smith, L. Spinoglio, and M. Wolfire. Observations of Arp 220 Using Herschel-SPIRE: An Unprecedented View of the Molecular Gas in an Extreme Star Formation Environment. *Astrophysical Journal*, 743:94, December 2011. doi: 10.1088/0004-637X/743/1/94.

G. H. Rieke, A. Alonso-Herrero, B. J. Weiner, P. G. Pérez-González, M. Blaylock, J. L. Donley, and D. Marcillac. Determining Star Formation Rates for Infrared Galaxies. *Astrophysical Journal*, 692:556–573, February 2009. doi: 10.1088/0004-637X/692/1/556.

I. G. Roseboom, J. S. Dunlop, M. Cirasuolo, J. E. Geach, I. Smail, M. Halpern, P. van der Werf, O. Almaini, V. Arumugam, V. Asboth, R. Auld, A. Blain, M. N. Bremer, J. Bock, R. A. A. Bowler, F. Buitrago, E. Chapin, S. Chapman, A. Chrysostomou, C. Clarke, A. Conley, K. E. K. Coppin, A. L. R. Danielson, D. Farrah, J. Glenn, E. Hatziminaoglou, E. Ibar, R. J. Ivison, T. Jenness, E. van Kampen, A. Karim, T. Mackenzie, G. Marsden, R. Meijerink, M. J. Michałowski, S. J. Oliver, M. J. Page, E. Pearson, D. Scott, J. M. Simpson, D. J. B. Smith, M. Spaans, A. M. Swinbank, M. Symeonidis, T. Targett, E. Valiante, M. Viero, L. Wang, C. J. Willott, and M. Zemcov. The SCUBA-2 Cosmology Legacy Survey: demographics of the 450-μm population. *Monthly Notices of the Royal Astronomical Society*, 436:430–448, November 2013. doi: 10.1093/mnras/stt1577.

D. B. Sanders, J. M. Mazzarella, D.-C. Kim, J. A. Surace, and B. T. Soifer. The IRAS Revised Bright Galaxy Sample. *Astronomical Journal*, 126: 1607–1664, October 2003. doi: 10.1086/376841.

K. S. Scott, J. E. Austermann, T. A. Perera, G. W. Wilson, I. Aretxaga, J. J. Bock, D. H. Hughes, Y. Kang, S. Kim, P. D. Mauskopf, D. B. Sanders, N. Scoville, and M. S. Yun. AzTEC millimetre survey of the COSMOS field - I. Data reduction and source catalogue. *Monthly Notices of the Royal Astronomical Society*, 385:2225–2238, April 2008. doi: 10.1111/j.1365-2966.2008.12989.x.

S. E. Scott, M. J. Fox, J. S. Dunlop, S. Serjeant, J. A. Peacock, R. J. Ivison, S. Oliver, R. G. Mann, A. Lawrence, A. Efstathiou, M. Rowan-Robinson, D. H. Hughes, E. N. Archibald, A. Blain, and M. Longair. The SCUBA 8-mJy survey - I. Submillimetre maps, sources and number counts. *Monthly Notices of the Royal Astronomical Society*, 331:817–838, April 2002. doi: 10.1046/j.1365-8711.2002.05193.x.

N. Scoville, H. Aussel, M. Brusa, P. Capak, C. M. Carollo, M. Elvis, M. Giavalisco, L. Guzzo, G. Hasinger, C. Impey, J.-P. Kneib, O. LeFevre, S. J. Lilly, B. Mobasher, A. Renzini, R. M. Rich, D. B. Sanders, E. Schinnerer, D. Schminovich, P. Shopbell, Y. Taniguchi, and N. D. Tyson. The

Cosmic Evolution Survey (COSMOS): Overview. *Astrophysical Journal Supplement*, 172:1–8, September 2007. doi: 10.1086/516585.

R. Siebenmorgen and E. Krügel. Dust in starburst nuclei and ULIRGs. SED models for observers. *Astronomy and Astrophysics*, 461:445–453, January 2007. doi: 10.1051/0004-6361:20065700.

R. F. Silverberg, M. G. Hauser, N. W. Boggess, T. J. Kelsall, S. H. Moseley, and T. L. Murdock. Design of the diffuse infrared background experiment (DIRBE) on COBE. In M. S. Scholl, editor, *Infrared Spaceborne Remote Sensing*, volume 2019 of *Proceedings of the SPIE*, pages 180–189, October 1993.

J. M. Simpson, A. M. Swinbank, I. Smail, D. M. Alexander, W. N. Brandt, F. Bertoldi, C. de Breuck, S. C. Chapman, K. E. K. Coppin, E. da Cunha, A. L. R. Danielson, H. Dannerbauer, T. R. Greve, J. A. Hodge, R. J. Ivison, A. Karim, K. K. Knudsen, B. M. Poggianti, E. Schinnerer, A. P. Thomson, F. Walter, J. L. Wardlow, A. Weiß, and P. P. van der Werf. An ALMA Survey of Submillimeter Galaxies in the Extended Chandra Deep Field South: The Redshift Distribution and Evolution of Submillimeter Galaxies. *Astrophysical Journal*, 788:125, June 2014. doi: 10.1088/0004-637X/788/2/125.

J. M. Simpson, I. Smail, A. M. Swinbank, O. Almaini, A. W. Blain, M. N. Bremer, S. C. Chapman, C.-C. Chen, C. Conselice, K. E. K. Coppin, A. L. R. Danielson, J. S. Dunlop, A. C. Edge, D. Farrah, J. E. Geach, W. G. Hartley, R. J. Ivison, A. Karim, C. Lani, C.-J. Ma, R. Meijerink, M. J. Michałowski, A. Mortlock, D. Scott, C. J. Simpson, M. Spaans, A. P. Thomson, E. van Kampen, and P. P. van der Werf. The SCUBA-2 Cosmology Legacy Survey: ALMA Resolves the Rest-frame Far-infrared Emission of Sub-millimeter Galaxies. *Astrophysical Journal*, 799:81, January 2015. doi: 10.1088/0004-637X/799/1/81.

J. M. Simpson, I. Smail, A. M. Swinbank, R. J. Ivison, J. S. Dunlop, J. E. Geach, O. Almaini, V. Arumugam, M. N. Bremer, C.-C. Chen, C. Conselice, K. E. K. Coppin, D. Farrah, E. Ibar, W. G. Hartley, C. J. Ma, M. J. Michałowski, D. Scott, M. Spaans, A. P. Thomson, and P. P. van der Werf. The SCUBA-2 Cosmology Legacy Survey: Multi-wavelength Properties of ALMA-identified Submillimeter Galaxies in UKIDSS UDS. *Astrophysical Journal*, 839:58, April 2017. doi: 10.3847/1538-4357/aa65d0.

G. Siringo, E. Kreysa, A. Kovács, F. Schuller, A. Weiß, W. Esch, H.-P. Gemünd, N. Jethava, G. Lundershausen, A. Colin, R. Güsten, K. M. Menten, A. Beelen, F. Bertoldi, J. W. Beeman, and E. E. Haller. The Large APEX BOlometer CAmera LABOCA. *Astronomy and Astrophysics*, 497:945–962, April 2009. doi: 10.1051/0004-6361/200811454.

V. Smolčić, M. Aravena, F. Navarrete, E. Schinnerer, D. A. Riechers, F. Bertoldi, C. Feruglio, A. Finoguenov, M. Salvato, M. Sargent, H. J. McCracken, M. Albrecht, A. Karim, P. Capak, C. L. Carilli, N. Cappelluti, M. Elvis, O. Ilbert, J. Kartaltepe, S. Lilly, D. Sanders, K. Sheth, N. Z. Scoville, and Y. Taniguchi. Millimeter imaging of submillimeter galaxies in the COSMOS field: redshift distribution. *Astronomy and Astrophysics*, 548:A4, December 2012. doi: 10.1051/0004-6361/201219368.

A. M. Swinbank, S. C. Chapman, I. Smail, C. Lindner, C. Borys, A. W. Blain, R. J. Ivison, and G. F. Lewis. The link between submillimetre galaxies and luminous ellipticals: near-infrared IFU spectroscopy of submillimetre galaxies. *Monthly Notices of the Royal Astronomical Society*, 371:465–476, September 2006. doi: 10.1111/j.1365-2966.2006.10673.x.

A. M. Swinbank, J. M. Simpson, I. Smail, C. M. Harrison, J. A. Hodge, A. Karim, F. Walter, D. M. Alexander, W. N. Brandt, C. de Breuck, E. da Cunha, S. C. Chapman, K. E. K. Coppin, A. L. R. Danielson, H. Dannerbauer, R. Decarli, T. R. Greve, R. J. Ivison, K. K. Knudsen, C. D. P. Lagos, E. Schinnerer, A. P. Thomson, J. L. Wardlow, A. Weiß, and P. van der Werf. An ALMA survey of sub-millimetre Galaxies in the Extended Chandra Deep Field South: the far-infrared properties of SMGs. *Monthly Notices of the Royal Astronomical Society*, 438:1267–1287, February 2014. doi: 10.1093/mnras/stt2273.

L. J. Tacconi, R. Genzel, I. Smail, R. Neri, S. C. Chapman, R. J. Ivison, A. Blain, P. Cox, A. Omont, F. Bertoldi, T. Greve, N. M. Förster Schreiber, S. Genel, D. Lutz, A. M. Swinbank, A. E. Shapley, D. K. Erb, A. Cimatti, E. Daddi, and A. J. Baker. Submillimeter Galaxies at z ˜ 2: Evidence for Major Mergers and Constraints on Lifetimes, IMF, and CO-H_2 Conversion Factor. *Astrophysical Journal*, 680:246-262, June 2008. doi: 10.1086/587168.

T. A. Targett, J. S. Dunlop, M. Cirasuolo, R. J. McLure, V. A. Bruce, A. Fontana, A. Galametz, D. Paris, R. Davé, A. Dekel, S. M. Faber, H. C. Ferguson, N. A. Grogin, J. S. Kartaltepe, D. D. Kocevski, A. M.

Koekemoer, P. Kurczynski, K. Lai, and J. Lotz. The properties of (sub-)millimetre-selected galaxies as revealed by CANDELS HST WFC3/IR imaging in GOODS-South. *Monthly Notices of the Royal Astronomical Society*, 432:2012–2042, July 2013. doi: 10.1093/mnras/stt482.

the ALMA Cycle 5 Technical Handbook. the alma cycle 5 technical handbook, 2017.

S. Toft, V. Smolčić, B. Magnelli, A. Karim, A. Zirm, M. Michalowski, P. Capak, K. Sheth, K. Schawinski, J.-K. Krogager, S. Wuyts, D. Sanders, A. W. S. Man, D. Lutz, J. Staguhn, S. Berta, H. Mccracken, J. Krpan, and D. Riechers. Submillimeter Galaxies as Progenitors of Compact Quiescent Galaxies. *Astrophysical Journal*, 782:68, February 2014. doi: 10.1088/0004-637X/782/2/68.

E. Valiante, M. W. L. Smith, S. Eales, S. J. Maddox, E. Ibar, R. Hopwood, L. Dunne, P. J. Cigan, S. Dye, E. Pascale, E. E. Rigby, N. Bourne, C. Furlanetto, and R. J. Ivison. The Herschel-ATLAS data release 1 - I. Maps, catalogues and number counts. *Monthly Notices of the Royal Astronomical Society*, 462:3146–3179, November 2016. doi: 10.1093/mnras/stw1806.

P. G. van Dokkum, E. J. Nelson, M. Franx, P. Oesch, I. Momcheva, G. Brammer, N. M. Förster Schreiber, R. E. Skelton, K. E. Whitaker, A. van der Wel, R. Bezanson, M. Fumagalli, G. D. Illingworth, M. Kriek, J. Leja, and S. Wuyts. Forming Compact Massive Galaxies. *Astrophysical Journal*, 813:23, November 2015. doi: 10.1088/0004-637X/813/1/23.

W.-H. Wang, L. L. Cowie, and A. J. Barger. An 850 Micron SCUBA Survey of the Hubble Deep Field-North GOODS Region. *Astrophysical Journal*, 613:655–671, October 2004. doi: 10.1086/423232.

W.-H. Wang, L. L. Cowie, A. J. Barger, and J. P. Williams. SMA Observations of GOODS 850-11 and GOODS 850-13: First Examples of Multiple Submillimeter Sources Resolved by an Interferometer. *Astrophysical Journal Letters*, 726:L18, January 2011. doi: 10.1088/2041-8205/726/2/L18.

J. L. Wardlow, I. Smail, K. E. K. Coppin, D. M. Alexander, W. N. Brandt, A. L. R. Danielson, B. Luo, A. M. Swinbank, F. Walter, A. Weiß, Y. Q. Xue, S. Zibetti, F. Bertoldi, A. D. Biggs, S. C. Chapman, H. Dannerbauer, J. S. Dunlop, E. Gawiser, R. J. Ivison, K. K. Knudsen, A. Kovács, C. G. Lacey, K. M. Menten, N. Padilla, H.-W. Rix, and P. P. van der

Werf. The LABOCA survey of the Extended Chandra Deep Field-South: a photometric redshift survey of submillimetre galaxies. *Monthly Notices of the Royal Astronomical Society*, 415:1479–1508, August 2011. doi: 10.1111/j.1365-2966.2011.18795.x.

A. Weiß, A. Kovács, K. Coppin, T. R. Greve, F. Walter, I. Smail, J. S. Dunlop, K. K. Knudsen, D. M. Alexander, F. Bertoldi, W. N. Brandt, S. C. Chapman, P. Cox, H. Dannerbauer, C. De Breuck, E. Gawiser, R. J. Ivison, D. Lutz, K. M. Menten, A. M. Koekemoer, E. Kreysa, P. Kurczynski, H.-W. Rix, E. Schinnerer, and P. P. van der Werf. The Large Apex Bolometer Camera Survey of the Extended Chandra Deep Field South. *Astrophysical Journal*, 707:1201–1216, December 2009. doi: 10.1088/0004-637X/707/2/1201.

G. W. Wilson, J. E. Austermann, T. A. Perera, K. S. Scott, P. A. R. Ade, J. J. Bock, J. Glenn, S. R. Golwala, S. Kim, Y. Kang, D. Lydon, P. D. Mauskopf, C. R. Predmore, C. M. Roberts, K. Souccar, and M. S. Yun. The AzTEC mm-wavelength camera. *Monthly Notices of the Royal Astronomical Society*, 386:807–818, May 2008. doi: 10.1111/j.1365-2966.2008.12980.x.

A. Wootten and A. R. Thompson. The Atacama Large Millimeter/Submillimeter Array. *IEEE Proceedings*, 97:1463–1471, August 2009. doi: 10.1109/JPROC.2009.2020572.

J. D. Younger, G. G. Fazio, J.-S. Huang, M. S. Yun, G. W. Wilson, M. L. N. Ashby, M. A. Gurwell, K. Lai, A. B. Peck, G. R. Petitpas, D. J. Wilner, D. Iono, K. Kohno, R. Kawabe, D. H. Hughes, I. Aretxaga, T. Webb, A. Martínez-Sansigre, S. Kim, K. S. Scott, J. Austermann, T. Perera, J. D. Lowenthal, E. Schinnerer, and V. Smolčić. Evidence for a Population of High-Redshift Submillimeter Galaxies from Interferometric Imaging. *Astrophysical Journal*, 671:1531–1537, December 2007. doi: 10.1086/522776.

J. D. Younger, G. G. Fazio, J.-S. Huang, M. S. Yun, G. W. Wilson, M. L. N. Ashby, M. A. Gurwell, A. B. Peck, G. R. Petitpas, D. J. Wilner, D. H. Hughes, I. Aretxaga, S. Kim, K. S. Scott, J. Austermann, T. Perera, and J. D. Lowenthal. The AzTEC/SMA Interferometric Imaging Survey of Submillimeter-selected High-redshift Galaxies. *Astrophysical Journal*, 704:803–812, October 2009. doi: 10.1088/0004-637X/704/1/803.

Appendix A

Data tables

Here we provide data tables detailing our interferometric sample. Each of the five fields used in our study are summarized in a single table. The columns give the source name, the SCUBA-2 position, the SMA (or ALMA) position, the SCUBA-2 observed flux density, the deboosted SCUBA-2 flux density, the SMA (or ALMA) observed flux density and the SMA deboosted flux density. For SMA pointings that did not detect any galaxies above 4σ we provide flux density upper limits. For sources that were deboosted to 0 mJy, we also provide 4σ upper limits. All sources are sorted by their deboosted SCUBA-2 flux density. We have used ALMA data from Simpson et al. (2015) for some of the sources in the UDS field; these sources are marked with a [b]. We have also used SMA data from Younger et al. (2007) and Younger et al. (2009) for some of the sources in the COSMOS field; these sources are marked with a [c] and a [d], respectively.

Table A.1: SMA sample plus archival ALMA data for the UDS field. Sources observed by ALMA in Simpson et al. (2015) are indicated by a [b], and all other sources were observed by the SMA in this work.

Source	RA/Dec SCUBA-2	RA/Dec SMA	$S^{\rm obs}_{\rm S2}$ [mJy]	$S_{\rm S2}$ [mJy]	$S^{\rm obs}_{\rm SMA}$ [mJy] ($S^{\rm obs}_{\rm ALMA}$)	$S_{\rm SMA}$ [mJy] ($S_{\rm ALMA}$)
Orochi[a]	02:18:30.77 −05:31:30.8	02:18:30.68 −05:31:31.7	52.7 ± 0.9	52.7 ± 1.2	90.7 ± 20.7	N/A
UDS156.0[b]	02:18:24.33 −05:22:56.8	02:18:24.14 −05:22:55.3	16.7 ± 0.9	16.4 ± 1.3	9.7 ± 0.7	9.7 ± 0.7
156.1[b]	02:18:24.33 −05:22:56.8	02:18:24.24 −05:22:56.9	16.7 ± 0.9	16.4 ± 1.3	8.5 ± 0.7	8.5 ± 0.7
UDS57.0[b]	02:19:21.19 −04:56:52.5	02:19:21.14 −04:56:51.3	13.0 ± 0.9	12.8 ± 1.7	9.5 ± 0.6	9.5 ± 0.6
57.1[b]	02:19:21.19 −04:56:52.5	02:19:20.88 −04:56:52.9	13.0 ± 0.9	12.8 ± 1.7	6.0 ± 0.9	5.8 ± 0.9
57.2[b]	02:19:21.19 −04:56:52.5	02:19:21.41 −04:56:49.0	13.0 ± 0.9	12.8 ± 1.7	1.8 ± 0.6	1.5 ± 0.6
57.3[b]	02:19:21.19 −04:56:52.5	02:19:21.39 −04:56:38.8	13.0 ± 0.9	12.8 ± 1.7	2.7 ± 1.0	2.1 ± 1.0
UDS03	02:15:55.41 −05:24:56.2	02:15:55.10 −05:24:56.6	12.8 ± 1.3	12.0 ± 1.8	13.7 ± 1.4	$13.1^{+1.2}_{-1.5}$
UDS361.0[b]	02:16:48.08 −05:01:30.7	02:16:47.92 −05:01:29.8	11.5 ± 0.9	11.3 ± 1.7	11.8 ± 0.6	11.8 ± 0.6
361.1[b]	02:16:48.08 −05:01:30.7	02:16:47.73 −05:01:25.8	11.5 ± 0.9	11.3 ± 1.7	2.6 ± 0.7	2.0 ± 0.7
UDS286.0[b]	02:17:25.81 −05:25:36.9	02:17:25.73 −05:25:41.2	11.4 ± 0.9	11.2 ± 1.7	5.2 ± 0.7	5.1 ± 0.7
286.1[b]	02:17:25.81 −05:25:36.9	02:17:25.63 −05:25:33.7	11.4 ± 0.9	11.2 ± 1.7	5.1 ± 0.6	5.0 ± 0.6
286.2[b]	02:17:25.81 −05:25:36.9	02:17:25.80 −05:25:37.5	11.4 ± 0.9	11.2 ± 1.7	2.7 ± 0.6	2.6 ± 0.6
286.3[b]	02:17:25.81 −05:25:36.9	02:17:25.52 −05:25:36.7	11.4 ± 0.9	11.2 ± 1.7	1.7 ± 0.6	1.4 ± 0.6
UDS269.0[b]	02:17:30.50 −05:19:22.9	02:17:30.44 −05:19:22.4	11.0 ± 0.9	10.7 ± 1.4	12.9 ± 0.6	12.9 ± 0.6
269.1[b]	02:17:30.50 −05:19:22.9	02:17:30.25 −05:19:18.4	11.0 ± 0.9	10.7 ± 1.4	2.6 ± 0.7	2.1 ± 0.7
UDS08	02:15:56.03 −04:55:10.3	02:15:55.95 −04:55:08.6	10.9 ± 1.0	10.5 ± 1.3	10.1 ± 1.7	$8.9^{+1.6}_{-1.6}$
UDS204.0[b]	02:18:03.04 −05:28:42.9	02:18:03.01 −05:28:41.9	10.7 ± 0.9	10.4 ± 1.2	11.6 ± 0.6	11.6 ± 0.6
204.1[b]	02:18:03.04 −05:28:42.9	02:18:03.01 −05:28:32.5	10.7 ± 0.9	10.4 ± 1.2	2.9 ± 0.9	2.2 ± 0.9
UDS202.0[b]	02:18:05.71 −05:10:50.9	02:18:05.65 −05:10:49.6	11.0 ± 0.9	10.4 ± 1.5	10.5 ± 0.5	10.5 ± 0.5
202.1[b]	02:18:05.71 −05:10:50.9	02:18:05.05 −05:10:46.3	11.0 ± 0.9	10.4 ± 1.5	3.9 ± 0.9	3.5 ± 0.9
UDS09	02:17:38.95 −04:33:37.0	02:17:38.82 −04:33:34.1	10.9 ± 1.3	10.1 ± 1.2	13.9 ± 0.8	$13.6^{+0.9}_{-0.7}$
UDS11	02:16:43.77 −05:17:54.7	02:16:43.72 −05:17:53.5	10.1 ± 0.9	9.8 ± 1.4	10.0 ± 1.8	$8.6^{+1.7}_{-1.5}$
UDS306.0[b]	02:17:17.23 −05:33:26.8	02:17:17.07 −05:33:26.6	9.9 ± 1.0	9.7 ± 1.3	8.3 ± 0.5	8.3 ± 0.5
306.1[b]	02:17:17.23 −05:33:26.8	02:17:17.16 −05:33:32.5	9.9 ± 1.0	9.7 ± 1.3	2.6 ± 0.4	2.3 ± 0.4
306.2[b]	02:17:17.23 −05:33:26.8	02:17:16.81 −05:33:31.8	9.9 ± 1.0	9.7 ± 1.3	3.0 ± 0.9	2.3 ± 0.9
UDS14	02:16:30.77 −05:24:02.6	Undetected	9.6 ± 0.9	9.4 ± 1.2	< 6.1	
UDS15	02:18:03.57 −04:55:26.9	Undetected	9.6 ± 0.9	9.4 ± 1.3	< 5.1	
UDS16	02:19:02.24 −05:28:56.6	02:19:02.05 −05:28:56.7	9.5 ± 1.0	9.3 ± 1.4	6.5 ± 1.5	$6.1^{+1.3}_{-1.6}$
UDS18	02:17:44.29 −05:20:08.9	02:17:44.22 −05:20:09.8	9.3 ± 0.9	9.1 ± 1.3	8.9 ± 1.5	$8.1^{+1.3}_{-1.4}$
UDS13	02:19:27.31 −04:45:08.5	02:19:27.17 −04:45:06.1	9.8 ± 1.1	9.0 ± 1.6	15.3 ± 1.1	$14.9^{+1.0}_{-1.2}$
UDS109.0[b]	02:18:50.32 −05:27:22.7	02:18:50.07 −05:27:25.5	9.4 ± 0.9	9.0 ± 1.5	7.7 ± 0.7	7.6 ± 0.7
109.1[b]	02:18:50.32 −05:27:22.7	02:18:50.30 −05:27:17.2	9.4 ± 0.9	9.0 ± 1.5	4.3 ± 0.6	4.2 ± 0.6
UDS48.0[b]	02:19:24.66 −04:53:00.5	02:19:24.57 −04:53:00.2	8.9 ± 0.8	8.9 ± 1.3	7.5 ± 0.5	7.5 ± 0.5
48.1[b]	02:19:24.66 −04:53:00.5	02:19:24.62 −04:52:56.9	8.9 ± 0.8	8.9 ± 1.3	1.6 ± 0.5	1.4 ± 0.5

Continued on next page

Table A.1 – continued from previous page

Source	RA/Dec SCUBA-2	RA/Dec SMA	$S^{\rm obs}_{\rm S2}$ [mJy]	$S_{\rm S2}$ [mJy]	$S^{\rm obs}_{\rm SMA}$ [mJy] ($S^{\rm obs}_{\rm ALMA}$)	$S_{\rm SMA}$ [mJy] ($S_{\rm ALMA}$)
UDS20	02:17:30.51 −04:59:36.9	02:17:30.61 −04:59:36.8	9.1 ± 0.9	8.7 ± 1.4	9.0 ± 1.4	$8.2^{+1.3}_{-1.3}$
UDS199.0[b]	02:18:07.31 −04:44:12.9	02:18:07.18 −04:44:13.8	9.2 ± 0.9	8.5 ± 1.4	4.3 ± 0.6	4.2 ± 0.6
199.1[b]	02:18:07.31 −04:44:12.9	02:18:07.19 −04:44:10.9	9.2 ± 0.9	8.5 ± 1.4	2.5 ± 0.5	2.4 ± 0.5
UDS22	02:16:11.81 −05:00:54.5	02:16:11.72 −05:00:54.0	9.0 ± 0.8	8.5 ± 1.2	15.0 ± 1.4	$14.1^{+1.5}_{-1.3}$
UDS160.0[b]	02:18:23.79 −05:11:40.9	02:18:23.73 −05:11:38.5	8.8 ± 0.9	8.4 ± 1.4	7.9 ± 0.6	7.9 ± 0.6
UDS110.0[b]	02:18:48.43 −05:18:06.7	02:18:48.24 −05:18:05.2	8.4 ± 0.9	8.2 ± 1.4	7.7 ± 0.6	7.7 ± 0.6
110.1[b]	02:18:48.43 −05:18:06.7	02:18:48.76 −05:18:02.1	8.4 ± 0.9	8.2 ± 1.4	2.5 ± 0.8	2.0 ± 0.8
UDS21	02:19:34.14 −04:44:40.4	02:19:34.15 −04:44:38.1	9.0 ± 1.2	8.2 ± 1.5	10.3 ± 1.0	$9.9^{+0.9}_{-1.0}$
UDS337.0[b]	02:16:41.11 −05:03:52.7	02:16:41.11 −05:03:51.4	8.4 ± 0.9	8.0 ± 1.2	8.1 ± 0.5	8.1 ± 0.5
UDS29	02:17:39.87 −05:29:18.9	02:17:39.78 −05:29:19.1	8.3 ± 0.9	8.0 ± 1.3	11.6 ± 1.1	$11.2^{+1.0}_{-1.2}$
UDS79.0[b]	02:19:10.09 −05:00:08.6	02:19:09.94 −05:00:08.6	8.1 ± 0.9	7.9 ± 1.4	7.7 ± 0.5	7.7 ± 0.5
UDS30	02:17:55.27 −04:47:22.9	02:17:55.05 −04:47:22.9	8.3 ± 0.9	7.8 ± 1.2	7.4 ± 1.1	$7.1^{+1.0}_{-1.0}$
UDS28	02:19:42.53 −05:18:04.3	02:19:42.45 −05:18:03.6	8.4 ± 1.1	7.6 ± 1.6	9.0 ± 1.0	$8.6^{+0.9}_{-1.0}$
UDS36	02:17:12.19 −04:43:18.9	02:17:12.21 −04:43:16.5	8.0 ± 0.9	7.6 ± 1.2	8.5 ± 1.4	$7.8^{+1.3}_{-1.2}$
UDS34	02:17:42.15 −04:56:28.9	02:17:41.92 −04:56:29.8	8.0 ± 0.9	7.6 ± 1.3	7.9 ± 1.2	$7.6^{+1.0}_{-1.3}$
UDS35	02:16:40.43 −05:13:38.7	02:16:40.40 −05:13:35.9	8.0 ± 0.9	7.6 ± 1.3	7.1 ± 1.4	$6.6^{+1.3}_{-1.4}$
UDS37	02:16:38.44 −05:01:22.7	02:16:38.33 −05:01:21.4	7.9 ± 0.9	7.5 ± 1.3	8.4 ± 1.3	$7.8^{+1.2}_{-1.2}$
UDS39	02:16:40.57 −05:11:00.7	02:16:40.59 −05:10:58.8	7.9 ± 0.9	7.5 ± 1.4	7.9 ± 1.0	$7.6^{+0.9}_{-1.0}$
UDS40	02:17:27.43 −05:06:44.9	02:17:27.29 −05:06:42.8	7.8 ± 0.9	7.5 ± 1.2	6.9 ± 1.1	$6.6^{+1.1}_{-1.0}$
UDS168.0[b]	02:18:20.46 −05:31:44.8	02:18:20.40 −05:31:43.2	8.2 ± 0.9	7.5 ± 1.4	6.7 ± 0.6	6.7 ± 0.6
168.1[b]	02:18:20.46 −05:31:44.8	02:18:20.31 −05:31:41.7	8.2 ± 0.9	7.5 ± 1.4	3.0 ± 0.6	2.8 ± 0.6
168.2[b]	02:18:20.46 −05:31:44.8	02:18:20.17 −05:31:38.6	8.2 ± 0.9	7.5 ± 1.4	2.0 ± 0.7	1.6 ± 0.7
UDS33	02:15:46.99 −05:18:52.2	02:15:46.70 −05:18:49.2	8.1 ± 1.2	7.4 ± 1.4	10.3 ± 1.0	$9.9^{+1.0}_{-1.0}$
UDS218.0[b]	02:17:54.87 −05:23:22.9	02:17:54.80 −05:23:23.0	7.6 ± 0.9	7.2 ± 1.3	6.6 ± 0.7	6.6 ± 0.7
UDS38	02:16:46.07 −05:03:46.7	02:16:46.17 −05:03:48.9	7.9 ± 0.9	7.2 ± 1.3	6.9 ± 1.6	$6.3^{+1.5}_{-1.5}$

[a] From Ikarashi et al. (2011) using the SMA at 860 μm.
[b] From Simpson et al. (2015) using ALMA at 870 μm, following the naming convention in their paper.

Table A.2: SMA sample for the SSA22 field. All observations are from this work.

Source	RA/Dec SCUBA-2	RA/Dec SMA	$S^{\rm obs}_{\rm S2}$ [mJy]	$S_{\rm S2}$ [mJy]	$S^{\rm obs}_{\rm SMA}$ [mJy]	$S_{\rm SMA}$ [mJy]
SSA22-01	22:17:32.50 +00:17:40.4	22:17:32.43 +00:17:44.1	14.5 ± 1.1	14.5 ± 1.4	12.2 ± 1.8	$10.6^{+1.9}_{-1.8}$
SSA22-03	22:16:56.10 +00:28:44.4	Undetected	11.1 ± 1.2	10.7 ± 1.4	<8.7	
SSA22-02	22:16:59.96 +00:10:40.4	22:16:59.83 +00:10:37.1	10.8 ± 1.1	10.2 ± 1.5	9.3 ± 1.6	$8.2^{+1.5}_{-1.6}$
SSA22-04	22:16:51.43 +00:18:20.4	Undetected	10.4 ± 1.1	10.0 ± 1.4	<12.6	
SSA22-08	22:18:06.63 +00:05:20.4	22:18:06.60 +00:05:20.5	10.0 ± 1.3	8.8 ± 1.8	9.5 ± 1.6	$8.2^{+1.7}_{-1.3}$
SSA22-07	22:17:18.90 +00:18:06.4	Undetected	8.5 ± 1.1	7.9 ± 1.3	<8.5	
SSA22-06	22:18:06.36 +00:11:34.4	22:18:06.48 +00:11:34.7	8.3 ± 1.1	7.7 ± 1.5	9.9 ± 1.3	$9.2^{+1.3}_{-1.3}$
SSA22-05	22:17:34.10 +00:13:52.4	22:17:33.90 +00:13:52.3	7.9 ± 1.1	7.3 ± 1.1	11.7 ± 2.0	$9.9^{+2.0}_{-1.8}$
SSA22-09	22:17:42.23 +00:17:00.4	Undetected	6.7 ± 1.1	6.0 ± 1.4	<8.5	

Table A.3: SMA sample plus archival SMA data for the COSMOS field. Sources observed by the SMA in Younger et al. (2007) are indicated by a [c], sources observed by the SMA in Younger et al. (2009) are indicated by a [d], and all other sources were observed by the SMA in this work. Flux density measurements from Younger et al. (2007) and Younger et al. (2009) were not deboosted. Values of N/A in the $S_{\rm SMA}$ column indicate sources where our deboosting simulation was not applicable.

Source	RA/Dec SCUBA-2	RA/Dec SMA	$S^{\rm obs}_{\rm S2}$ [mJy]	$S_{\rm S2}$ [mJy]	$S^{\rm obs}_{\rm SMA}$ [mJy]	$S_{\rm SMA}$ [mJy]
AzTEC1[c]	09:59:42.89 +02:29:36.5	09:59:42.86 +02:29:38.2	16.7 ± 1.5	16.0 ± 3.0	15.6 ± 1.1	
AzTEC2[c]	10:00:08.11 +02:26:12.6	10:00:08.05 +02:26:12.2	15.4 ± 1.4	14.7 ± 2.3	12.4 ± 1.0	
COSMOS05	09:59:22.99 +02:51:36.4	09:59:22.99 +02:51:36.4	14.0 ± 1.5	13.0 ± 1.7	13.7 ± 2.3	$11.3^{+2.4}_{-2.2}$
COSMOS06	09:58:42.40 +02:54:42.2	Undetected	14.0 ± 1.5	13.0 ± 2.1	<8.1	
COSMOS10	10:00:15.72 +02:15:48.6	10:00:15.72 +02:15:48.6	12.9 ± 0.8	12.9 ± 1.2	16.8 ± 1.5	$15.8^{+1.7}_{-1.5}$
COSMOS07[e]	09:58:37.92 +02:14:06.3	09:58:37.99 +02:14:08.5	13.2 ± 1.0	12.4 ± 1.5	13.8 ± 2.8	$10.7^{+2.4}_{-3.1}$
COSMOS09[e]	10:00:57.22 +02:20:12.6	10:00:57.22 +02:20:12.6	13.0 ± 1.5	12.1 ± 2.2	12.5 ± 2.5	$9.7^{+2.5}_{-2.3}$
AzTEC9[d]	09:59:57.44 +02:27:28.6	09:59:57.25 +02:27:30.6	12.4 ± 1.4	11.8 ± 1.9	9.0 ± 2.2	
COSMOS08	09:59:10.31 +02:48:54.4	09:59:10.34 +02:48:55.5	13.1 ± 1.6	11.7 ± 2.1	12.7 ± 2.0	$11.3^{+1.6}_{-2.3}$
COSMOS11a	09:58:45.89 +02:43:26.3	09:58:45.95 +02:43:29.1	12.5 ± 1.6	11.5 ± 2.0	8.6 ± 1.1	$8.0^{+1.1}_{-1.0}$
11b	09:58:45.89 +02:43:26.3	09:58:46.06 +02:43:31.5	12.5 ± 1.6	11.5 ± 2.0	5.1 ± 1.1	N/A
COSMOS15	09:57:49.03 +02:46:15.9	09:57:48.93 +02:46:19.9	11.8 ± 1.5	11.2 ± 2.1	11.2 ± 2.0	$9.7^{+1.6}_{-2.2}$
AzTEC5[c]	10:00:19.86 +02:32:04.6	10:00:19.75 +02:32:04.4	12.0 ± 1.4	11.2 ± 2.2	9.3 ± 1.3	
COSMOS14	10:00:13.46 +01:37:04.7	10:00:13.47 +01:37:04.3	12.0 ± 1.5	11.0 ± 1.8	12.2 ± 1.2	$11.7^{+1.0}_{-1.3}$
COSMOS17	10:00:04.78 +02:30:44.6	Undetected	11.2 ± 1.4	11.0 ± 1.8	<8.4	
AzTEC12[d]	10:00:35.34 +02:43:52.6	10:00:35.29 +02:43:53.4	11.6 ± 1.3	10.9 ± 2.0	13.5 ± 1.8	
COSMOS18	09:58:40.46 +02:05:14.4	09:58:40.28 +02:05:14.5	11.1 ± 1.5	10.4 ± 2.1	10.9 ± 1.7	$9.7^{+1.6}_{-1.7}$
AzTEC8[d]	09:59:59.44 +02:34:38.6	09:59:59.34 +02:34:41.0	10.9 ± 1.4	10.1 ± 1.8	19.7 ± 1.8	
AzTEC7[c]	10:00:17.99 +02:48:30.5	10:00:18.06 +02:48:30.5	10.8 ± 1.4	9.7 ± 2.0	12.0 ± 1.5	
COSMOS21	09:59:07.63 +02:58:36.3	09:59:07.49 +02:58:39.3	10.6 ± 1.5	9.5 ± 2.0	9.9 ± 1.9	$8.3^{+1.8}_{-1.8}$
AzTEC3[c]	10:00:20.79 +02:35:20.6	10:00:20.70 +02:35:20.5	9.2 ± 1.3	8.6 ± 1.5	8.7 ± 1.5	
AzTEC11.N[d]	10:00:08.91 +02:40:10.6	10:00:08.91 +02:40:09.6	9.3 ± 1.4	8.3 ± 1.8	10.0 ± 2.1	
11.S[d]	10:00:08.91 +02:40:10.6	10:00:08.94 +02:40:12.3	9.3 ± 1.4	8.3 ± 1.8	4.4 ± 2.1	
COSMOS23	10:00:10.12 +02:13:34.6	Undetected	8.4 ± 0.9	8.2 ± 1.4	<9.3	
AzTEC6[c]	10:00:06.64 +02:38:34.6	10:00:06.50 +02:38:37.7	8.9 ± 1.4	8.0 ± 1.8	8.6 ± 1.3	
AzTEC4[c]	09:59:31.68 +02:30:42.5	09:59:31.72 +02:30:44.0	9.3 ± 1.5	7.9 ± 1.9	14.4 ± 1.9	
COSMOS22	09:59:33.55 +02:23:46.5	09:59:33.55 +02:23:46.5	8.5 ± 1.2	7.8 ± 1.6	8.9 ± 2.2	$7.2^{+2.0}_{-7.2}$
COSMOS24	09:59:12.08 +02:09:54.5	09:59:12.17 +02:09:57.1	7.9 ± 1.1	7.2 ± 1.3	8.1 ± 1.7	$7.0^{+1.6}_{-1.6}$
COSMOS25	10:00:23.73 +02:19:14.6	Undetected	7.2 ± 1.0	7.1 ± 1.1	<9.3	
COSMOS01[f]		10:02:09.77 +02:36:33.9			10.6 ± 1.2	
COSMOS02[f]		10:02:49.19 +02:32:55.3			18.6 ± 0.7	

[c] From Younger et al. (2007) using the SMA at 890 μm, following the naming convention in their paper.
[d] From Younger et al. (2009) using the SMA at 890 μm, following the naming convention in their paper.
[e] Also detected with PdBI in Smolčić et al. (2012).
[f] Source is found in the CLS maps but outside the area defining the CLS catalogue, and hence not used in our analysis.

Table A.4: SMA sample for the LHN field. All observations are from this work. Values of N/A in the $S_{\rm SMA}$ column indicate sources where our deboosting simulation was not applicable.

Source	RA/Dec SCUBA-2	RA/Dec SMA	$S^{\rm obs}_{\rm S2}$ [mJy]	$S_{\rm S2}$ [mJy]	$S^{\rm obs}_{\rm SMA}$ [mJy]	$S_{\rm SMA}$ [mJy]
LHN01	10:46:45.01 +59:15:39.8	10:46:45.00 +59:15:41.6	12.3 ± 1.2	12.3 ± 1.8	10.3 ± 1.9	$8.8^{+1.8}_{-1.7}$
LHN02	10:46:35.78 +59:07:48.0	10:46:35.91 +59:07:48.1	12.0 ± 1.0	11.9 ± 1.2	12.2 ± 1.9	$10.4^{+2.0}_{-1.7}$
LHN03a	10:47:27.66 +58:52:14.6	10:47:27.97 +58:52:14.1	10.4 ± 1.1	9.9 ± 1.3	8.1 ± 1.8	$7.3^{+1.5}_{-1.8}$
03b	10:47:27.66 +58:52:14.6	10:47:26.52 +58:52:12.8	10.4 ± 1.1	9.9 ± 1.3	8.0 ± 1.9	$7.1^{+1.6}_{-1.9}$
LHN06	10:45:55.19 +59:15:28.1	10:45:55.24 +59:15:28.6	9.7 ± 1.1	9.7 ± 0.9	7.2 ± 1.8	$6.6^{+1.5}_{-6.5}$
LHN04	10:48:03.37 +58:54:22.9	10:48:03.57 +58:54:21.5	10.1 ± 1.3	8.9 ± 1.4	14.1 ± 2.4	$11.7^{+2.2}_{-2.5}$
LHN08	10:47:00.03 +59:01:07.5	10:47:00.18 +59:01:07.5	9.2 ± 1.0	8.9 ± 1.6	10.4 ± 1.6	$9.4^{+1.4}_{-1.6}$
LHN11*	10:45:22.55 +59:17:21.7	10:45:22.28 +59:17:25.6	8.6 ± 1.4	8.8 ± 1.7	7.0 ± 1.8	Undetected
LHN07	10:45:35.23 +58:50:49.9	10:45:34.98 +58:50:49.9	9.3 ± 1.1	8.7 ± 1.4	9.6 ± 1.6	$8.8^{+1.3}_{-1.6}$
LHN10	10:45:54.58 +58:47:54.1	10:45:54.50 +58:47:55.6	8.8 ± 1.1	8.3 ± 1.5	8.2 ± 0.8	$8.1^{+0.7}_{-0.8}$
LHN05	10:43:51.48 +59:00:57.7	10:43:51.21 +59:00:58.1	10.0 ± 1.5	8.2 ± 2.1	10.9 ± 2.4	$8.8^{+2.0}_{-2.3}$
LHN09a	10:45:23.87 +59:16:25.7	10:45:23.11 +59:16:18.6	9.0 ± 1.3	8.2 ± 1.5	9.4 ± 1.5	$8.6^{+1.3}_{-1.4}$
09b*	10:45:23.87 +59:16:25.7	10:45:25.01 +59:16:25.7	9.0 ± 1.3	8.2 ± 1.5	5.1 ± 1.5	N/A
09c*	10:45:23.87 +59:16:25.7	10:45:23.71 +59:16:31.9	9.0 ± 1.3	8.2 ± 1.5	4.5 ± 1.5	N/A
LHN12*	10:46:32.85 +59:02:12.0	10:46:32.80 +59:02:14.4	8.6 ± 1.0	8.1 ± 1.3	6.0 ± 2.0	Undetected
LHN13a	10:47:25.25 +59:03:40.7	10:47:25.47 +59:03:36.7	8.5 ± 1.1	7.9 ± 1.4	5.5 ± 0.8	N/A
13b	10:47:25.25 +59:03:40.7	10:47:25.13 +59:03:41.5	8.5 ± 1.1	7.9 ± 1.4	3.9 ± 0.8	N/A
LHN14	10:46:31.68 +58:50:54.0	10:46:31.58 +58:50:55.7	8.5 ± 1.1	7.9 ± 1.4	7.1 ± 0.8	$7.0^{+0.7}_{-0.8}$
LHN15	10:46:57.26 +59:14:57.6	10:46:57.30 +59:14:58.6	8.5 ± 1.2	7.9 ± 0.9	5.5 ± 0.7	$5.5^{+0.6}_{-0.8}$
LHN16	10:44:56.86 +58:49:59.0	10:44:56.74 +58:49:59.7	8.3 ± 1.1	7.6 ± 1.4	16.9 ± 2.5	$13.9^{+3.0}_{-2.2}$
LHN17	10:44:47.69 +59:00:36.6	10:44:47.68 +59:00:35.6	8.1 ± 1.1	7.5 ± 1.3	5.6 ± 0.7	$5.5^{+0.7}_{-0.7}$
LHN18	10:47:20.57 +59:10:40.9	10:47:20.54 +59:10:43.4	8.1 ± 1.1	7.3 ± 1.3	7.0 ± 0.8	$6.9^{+0.7}_{-0.7}$

* Source falls below the 4σ threshold in the SMA data, but a $>3\sigma$ peak has excellent positional alignment with IR and radio counterparts.

Table A.5: SMA sample for the EGS field. All observations are from this work.

Source	RA/Dec SCUBA-2	RA/Dec SMA	$S^{\rm obs}_{\rm S2}$ [mJy]	$S_{\rm S2}$ [mJy]	$S^{\rm obs}_{\rm SMA}$ [mJy]	$S_{\rm SMA}$ [mJy]
EGS01	14:19:51.56 +53:00:44.8	14:19:51.33 +53:00:46.4	16.3 ± 1.2	16.3 ± 1.4	13.2 ± 0.9	$12.9^{+0.9}_{-0.8}$
EGS02	14:15:57.62 +52:07:11.1	14:15:57.53 +52:07:12.7	12.7 ± 1.3	12.1 ± 1.2	13.8 ± 1.4	$12.9^{+1.5}_{-1.2}$
EGS03	14:15:47.46 +52:13:47.2	14:15:47.09 +52:13:48.6	10.8 ± 1.0	10.5 ± 1.1	16.4 ± 2.8	$12.9^{+2.9}_{-2.4}$
EGS05	14:19:20.35 +52:56:08.9	14:19:20.08 +52:56:09.1	10.7 ± 1.0	10.1 ± 1.4	20.0 ± 0.9	$19.7^{+1.0}_{-0.8}$
EGS06	14:17:40.55 +52:29:04.7	14:17:40.34 +52:29:06.7	10.0 ± 1.0	9.8 ± 2.3	9.8 ± 2.0	$8.9^{+1.7}_{-1.8}$
EGS08	14:19:00.37 +52:49:45.3	14:19:00.24 +52:49:48.3	10.4 ± 1.1	9.8 ± 1.5	8.6 ± 1.5	$8.1^{+1.5}_{-1.4}$
EGS04	14:19:14.54 +53:00:33.6	14:19:14.32 +53:00:33.8	10.5 ± 1.4	9.3 ± 1.6	11.1 ± 1.5	$10.5^{+1.2}_{-1.6}$
EGS10	14:17:44.09 +52:21:22.4	14:17:43.38 +52:21:21.7	10.2 ± 1.5	9.2 ± 2.3	8.3 ± 1.6	$7.7^{+1.6}_{-1.5}$
EGS11	14:17:41.73 +52:22:04.6	14:17:41.41 +52:22:07.9	9.8 ± 1.4	9.2 ± 1.4	7.2 ± 1.5	$6.7^{+1.6}_{-1.3}$
EGS07[f]		14:18:22.04 +52:54:02.0			7.7 ± 1.5	
EGS09[f]		14:20:52.55 +52:54:00.3			6.1 ± 1.4	

[f] Source is found in the CLS maps but outside the area defining the CLS catalogue, and hence not used in our analysis.

Appendix B

Multiwavelength cutouts

Here we provide *Spitzer*-IRAC 3.6 μm, *Spitzer*-MIPS 24 μm and VLA 1.4 GHz cutouts of the 38 sources for which these two images are available. Overlaid are SMA contours starting from 2σ in steps of 1σ.

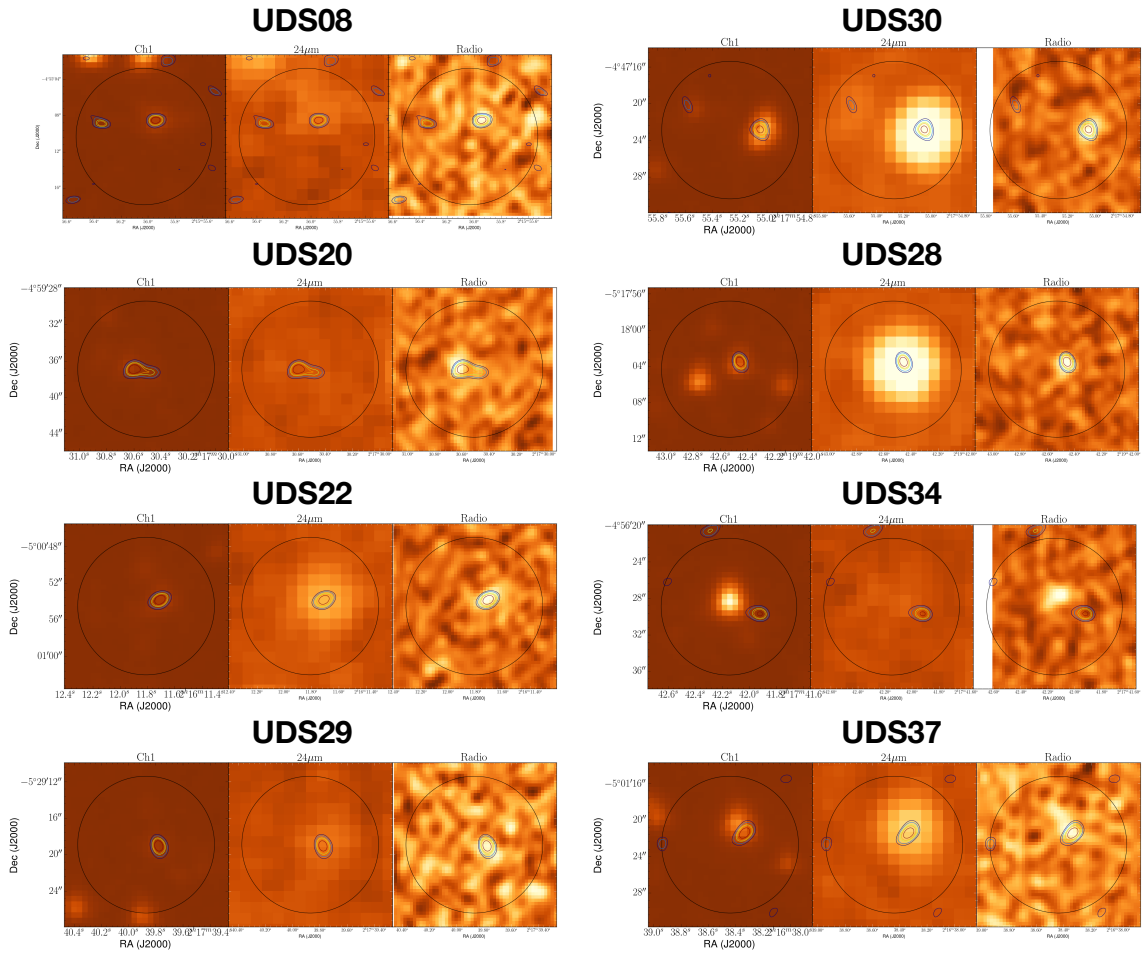

Figure B.1: Multiwavelength cut-outs of 38 sources in our sample with *Spitzer*-IRAC 3.6μm, *Spitzer*-MIPS 24μm and VLA 1.4 GHz imaging. We show SMA flux contours starting from 2σ in steps of 1σ overlaid over the IR and radio data.

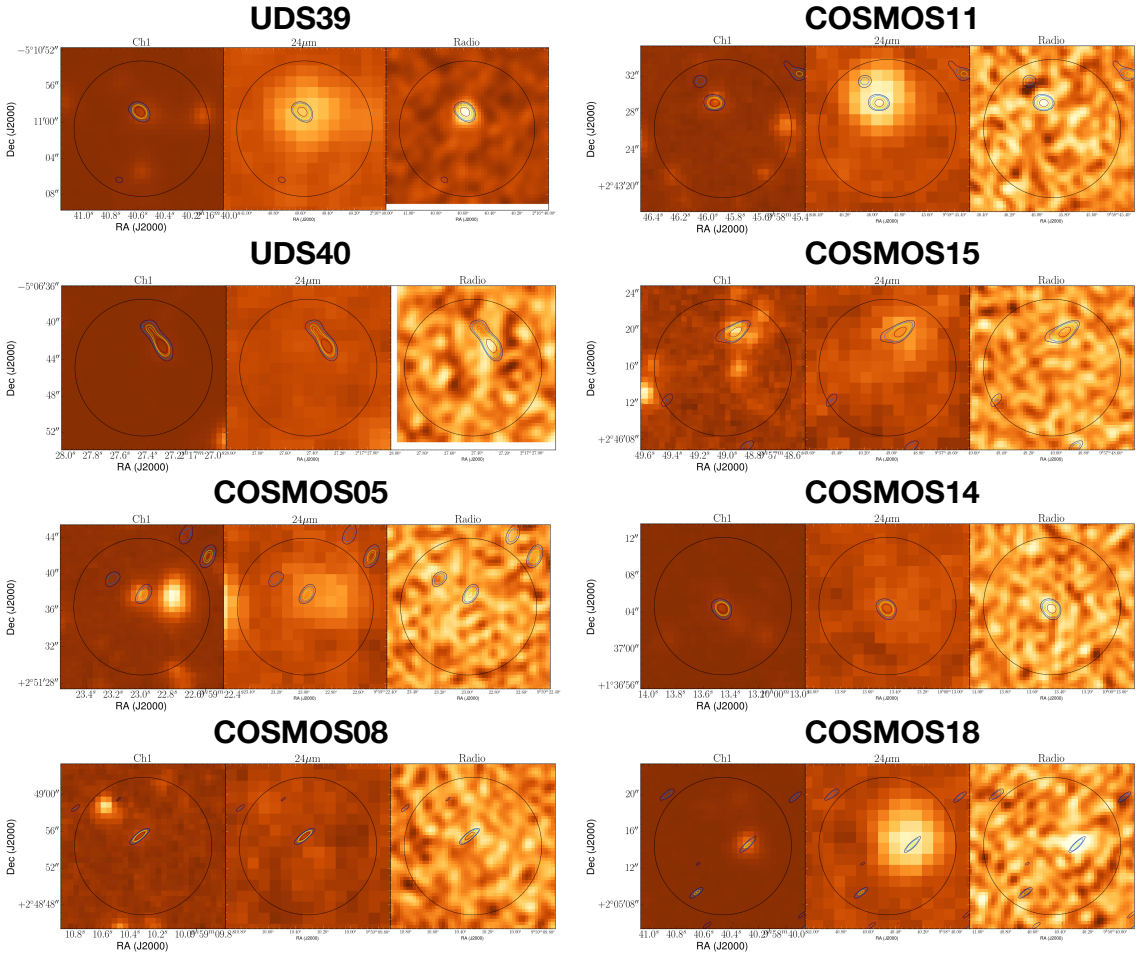

Figure B1 (Cont.)

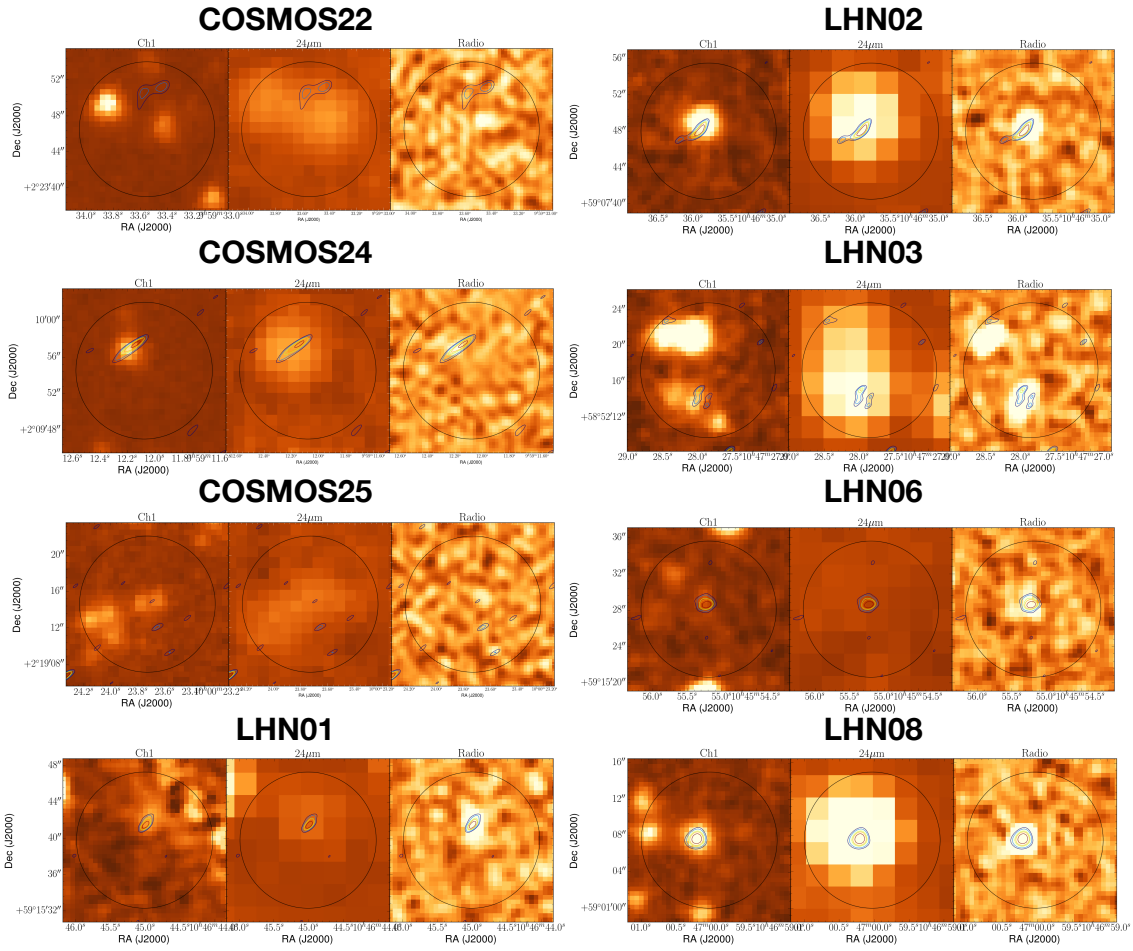

Figure B1 (Cont.)

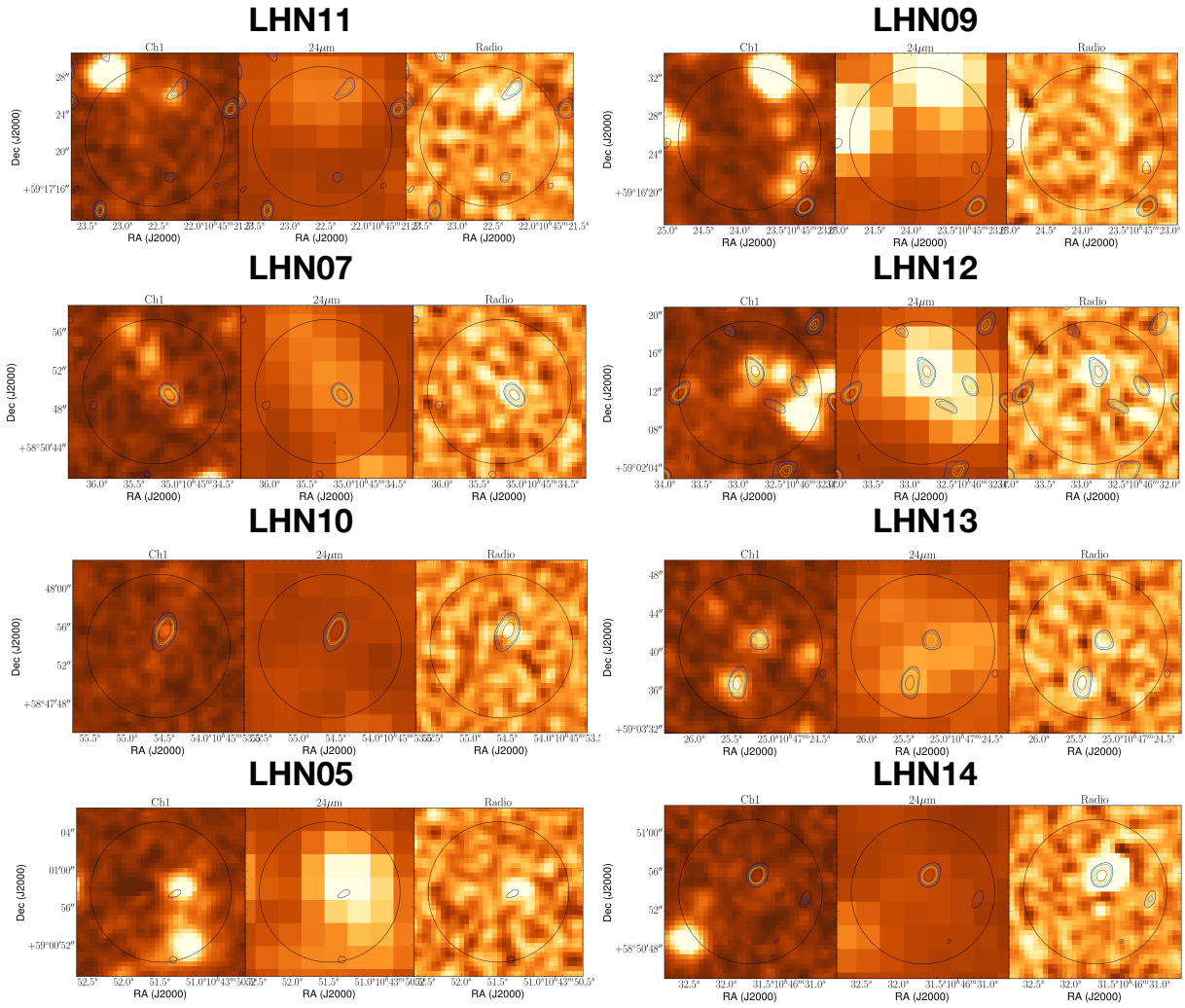

Figure B1 (Cont.)

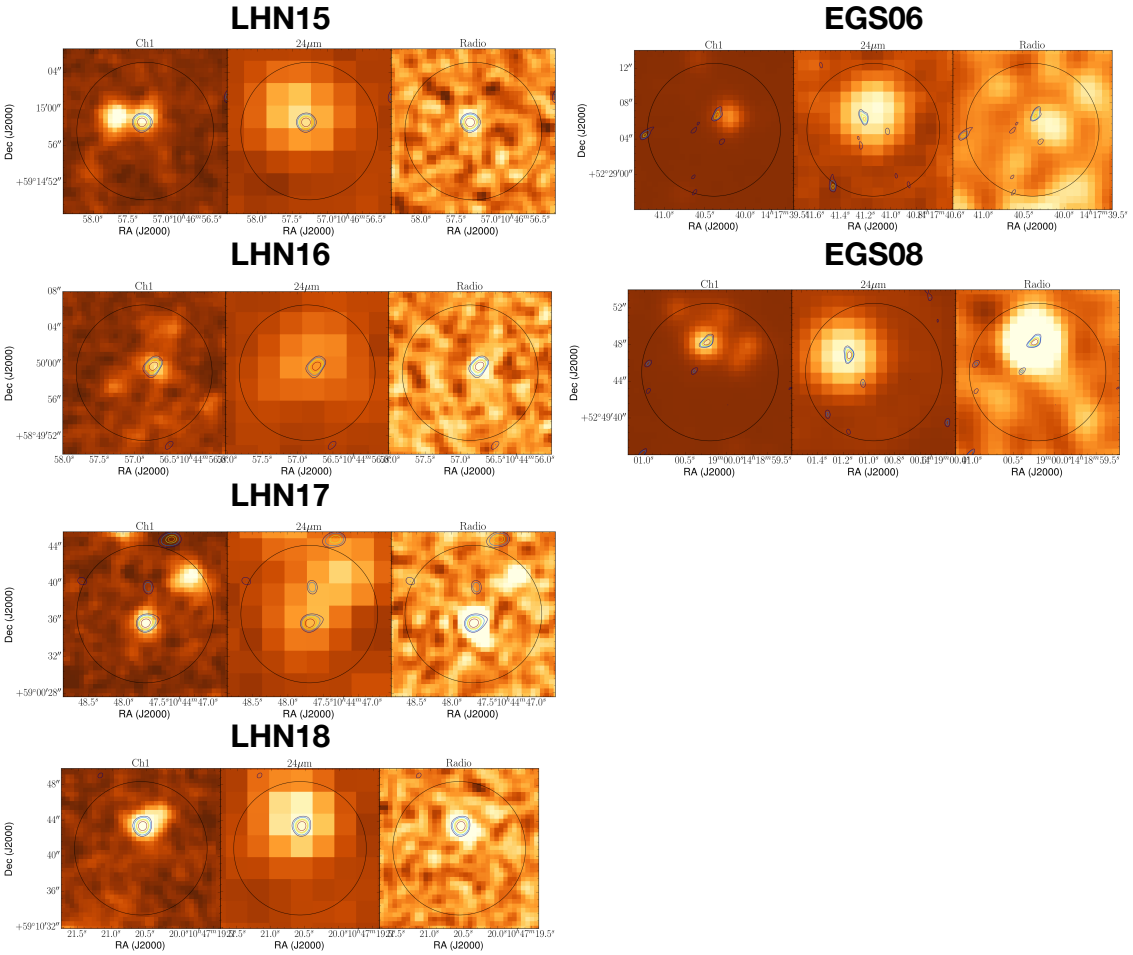

Figure B1 (Cont.)